ACS Catalysis

pubs.acs.org/acscatalysis Perspective

Atomically Dispersed Metal−Nitrogen−Carbon Catalysts for Electrochemical Nitrogen Transformations to Ammonia and Beyond

Eamonn Murphy, Yuanchao Liu, Baiyu Sun, Yu-Han Chen, Shengyuan Guo, and Plamen Atanassov*

Cite This: ACS Catal. 2024, 14, 9797−9811 Read Online

ACCESS | Metrics & More | Article Recommendations | Supporting Information

ABSTRACT: The electrochemical reduction of reactive nitrogen species plays a critical role in achieving a pathway for the carbon-neutral synthesis of ammonia (NH_3) and urea to produce synthetic fertilizers and as an energy storage vector. Atomically dispersed metal−nitrogen−carbon (M−N−C) catalysts have demonstrated great success in achieving efficient NH_3 synthesis due to their full atom utilization, unique reaction pathways, high level of tailorability, and selectivity to mononitrogen products. This perspective focuses on M−N−C catalysts for electrochemical nitrogen transformations, where original experimental results utilizing 15 atomically dispersed mono- and bimetallic M−N−Cs are rigorously evaluated and compared with the literature for the highly controversial dinitrogen reduction reaction (N_2RR). The current state for M−N−Cs applied for the reduction of nitrogen oxides (NO_3^-/NO_2^-), utilizing M−N−Cs both as the primary catalyst and as an active support, is discussed. Furthermore, the coreduction of NO_3^- and CO_2 for C−N bond formation is presented with an emphasis on approaches for accurate urea detection to avoid false positives. Several possible C−N coupling pathways over metal-free nitrogen moieties, monometallic (M−N_x), and bimetallic active (M_1−N_x + M_2−N_x and M_1−M_2−N_x) sites are discussed. Finally, an outlook discussing the most significant challenges and opportunities in each of the three N-transformation pathways is discussed.

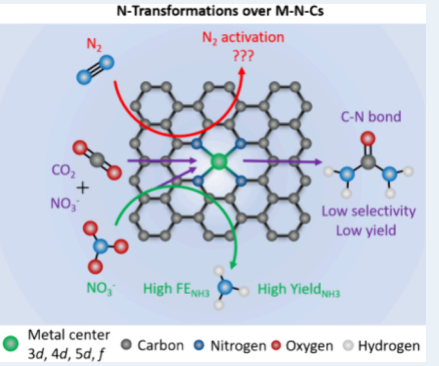

KEYWORDS: *nitrogen reduction, nitrate reduction, ammonia, urea, single atom catalyst*

INTRODUCTION

Extensive global research efforts have been devoted to the decarbonization of fuels and chemicals through carbon-neutral, electrochemical pathways.[1,2] A main focus of these research efforts is aimed at the reductive electrochemical transformation of oxygen (O_2, fuel cells), carbon dioxide (CO_2, high value chemicals), and nitrogen (N_2, ammonia production).[3−6] With carbon neutrality, electrochemical synthesis of ammonia (NH_3) from the nitrogen reduction reaction (N_2RR) remains among the most challenging transformations.[7,8]

Despite significant challenges, the N_2RR has received significant attention in the scientific community over the last several years, with over 2,000 peer-reviewed publications and extensive resources being devoted globally.[9] The worldwide funding investment in the decarbonization of NH_3 highlights its critical importance, as NH_3 is primarily used in the production of synthetic fertilizers, responsible for supporting the growing global population.[10] To date, the only industrialized method for large-scale NH_3 production remains the century-old Haber−Bosch (HB) process. The HB process is a thermal gas-phase reaction, which utilizes harsh reaction conditions (350−450 °C, 150−200 bar), making it energetically favorable to activate and dissociate the N_2, cleaving the very stable N≡N. Despite the great achievements of the HB process, it is extremely energy-intensive (harsh reaction conditions) and CO_2-emitting, due to the production of H_2, largely being gray H_2, sourced from steam reformation reactions.[5]

Therefore, alternative carbon-neutral pathways for NH_3 synthesis, such as mechanochemical, joule heating, and electrochemical approaches, have been investigated.[11,12] The most heavily researched approach is the electrochemical pathway due to its theoretical possibility to activate and reduce N_2 to NH_3 at ambient conditions.[8] While utilizing protons (H^+) from water-splitting reactions and renewable electrons (e^-), enabling the synthesis of a carbon-neutral NH_3 molecule. In practice, however, the direct activation of N_2 in aqueous protic conditions is extremely difficult and will be discussed explicitly in the N_2RR section. The challenges of N_2 activation have resulted in low NH_3 partial current densities (j_{NH3}), leading to extremely small amounts of NH_3 being produced. Combing the limited activity of the N_2RR, with ubiquitous NH_3 (or NO_x species) contamination present in N_2RR systems, results in the direct N_2RR remaining in an unviable state. Even to the extent that it has been reported that

Received: May 7, 2024
Revised: May 23, 2024
Accepted: June 4, 2024
Published: June 17, 2024

https://doi.org/10.1021/acscatal.4c02717
ACS Catal. 2024, 14, 9797−9811

the direct N_2RR in aqueous protic electrolytes remains unproven, despite the multitude of reports in the literature, as will be discussed and further evidenced with original experimental results.[13,14]

Although the direct activation of N_2 in aqueous electrolytes, synthesizing NH_3 from air and water is the goal of N_2 reduction, to circumvent the extreme challenges discussed earlier, alternative pathways are being researched as shown in Figure 1. For N_2 activation, via a $3e^-$ transfer reaction per NH_3

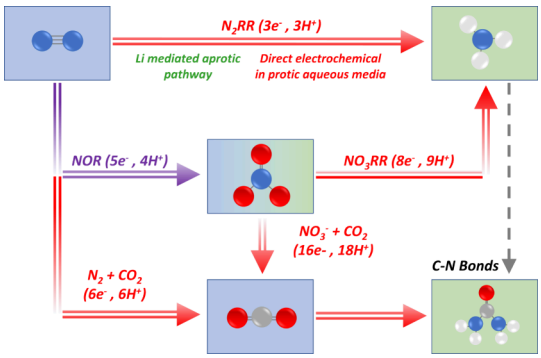

Figure 1. Electrochemical nitrogen transformation landscape to NH_3 through the N_2 and NO_3^- reduction pathways. An additional pathway for C−N bonds is shown by the simultaneous reduction of N_2/NO_3^- and CO_2. Reductive pathways are shown in red, and an oxidative pathway for NO_3^- production through N_2 is shown in purple. Blue circles indicate nitrogen, red circles indicate oxygen, gray circles indicate carbon, and white circles indicate hydrogen.

molecule, two pathways exist as shown in the top row of Figure 1. The direct N_2RR, which, in the opinion of several publications, remains unproven and irreproducible, or the confirmed, reproducible pathway, which follows a lithium-mediated approach in either a batchwise or continuous process. The Li-mediated approach has seen significant progress in recent years, resulting in near 100% FE to NH_3; however, it is still practically limited thermodynamically, in its energy efficiency due to the large overpotential required to plate the Li^+ to Li metal.[15−17] Recently, there has been a resurgence in the electrochemical reduction of nitrogen oxides, specifically nitrates (NO_3^-, NO_3RR) and nitrites (NO_2^-, NO_2RR) to NH_3 shown in the center of Figure 1,[18,19] where the nitrogen oxides can directly be the starting molecule, or N_2 can be oxidized to form NO_x species. This transformation requires either an $8e^-$ (NO_3^-) or $6e^-$ (NO_2^-) transfer per NH_3 molecule, as compared to the $3e^-$ for N_2. However, NO_x presents several advantages such as drastically increased solubility and favorable activation energies, enabling high NH_3 selectivity and yield rates, currently orders of magnitude larger than those of the other pathways. The use of highly soluble and active NO_x species synergizes well with gas-phase CO_2/CO, especially in gas diffusion electrode (GDE) configurations, enabling the coreduction of C and N species at the triple phase interface, for electrochemical C−N bond formation. The field of electrochemical C−N bond formation has gained significant interest over the last year, allowing for the direct synthesis of urea through an extremely complex $16e^-$ ($18H^+$) transfer reaction (CO_2 + NO_3^-), as shown in the bottom pathway of Figure 1.[20,21] Throughout this manuscript, each pathway will be thoroughly discussed in individual sections, highlighting achievements and challenges in each approach.

Atomically dispersed metal−nitrogen−carbon (M−N−C) catalysts have been widely explored and reported for the past several decades, beginning with macrocycles in the 1960s[22,23] and first gaining attention as potential platinum group metal (PGM) free catalysts for the oxygen reduction reaction (ORR) in fuel cells.[24−26] Aimed at reducing the required metal loading due to the significantly enhanced utilization of atomically dispersed metals compared to their nanoparticle counter parts, where even 2−3 nm particles utilize less than 50% of the atoms, buried under the surface.[27] With extensive research efforts, the tailorability of atomically dispersed catalysts, where the metal center and coordinating ligands can be optimized, the use of M−N−C catalysts has extended to the electrochemical CO_2 reduction reaction (CO_2RR), N_2RR, NO_3/NO_2RR, and even C−N bond formation.[14,28−32] Further research efforts have employed the use of multimetallic sites in a single bi- or trimetallic M−N−C, to selectively target reactant molecules or create cascade catalysis pathways for efficient electrochemical transformations.[32−34] A main disadvantage of M−N−C catalysts in N-transformation reactions arises due to the limiting weight percent of metal (usually sub 5 wt %) that can be utilized before nanoclusters or particles are formed, which can limit the total quantity of active sites available, often limiting reaction current densities. Recently, the applicability of M−N−C materials have been extended beyond a primary catalyst, but employed as an active support, where metallic nanoparticles are reduced onto an M−N−C, creating a hybrid nanoparticle/M−N−C catalyst.[35−38] The atomically dispersed $M-N_x$ sites not only add to the plurality of active sites increasing performance but also electronically alter the state of the nanoparticles, tailoring intermediate adsorption energies and increasing nanoparticle stability.

In this perspective, we utilized a set of 15 atomically dispersed mono and bimetallic M−N−C catalysts composed of 3d, 4d, 5d, and f metal centers (M = Cr, Mn, Fe, Co, Ni, Cu, Mo, Ru, Rh, Pd, W, La, Ce, FeMo, and FeCo) that have demonstrated significant NO_2^-/NO_3^- reduction activity (up to 100% efficiency) in a series of recent publications[34,35,39] and rigorously evaluated their N_2RR performance, revealing no successful N_2 activation, in contrast to the reported N_2RR literature. The application of M−N−C catalysts for the reduction of nitrogen oxides is then discussed, highlighting critical challenges in this rapidly progressing field such as energy efficiency. The feasibility and possible reaction pathways of C−N bond formation over metal-free N-moieties and mono- and bimetallic M−N−Cs both in a diatomic ($M_1-M_2-N_x$) and separate mono atomic (M_1-N_x + M_2-N_x) form are discussed. Importantly, errors with commonly employed urea detection methods are discussed. Finally, an outlook with the state of the field, achievements, and challenges is presented for each nitrogen transformation pathway.

M−N−C CATALYST SYNTHESIS

The set of atomically dispersed mono- and bimetallic M−N−C catalysts experimentally utilized in this study are synthesized via the sacrificial support method (SSM), which is a hard templating method that mixes a metal-containing precursor with a sacrificial nanoporous silica that can be removed upon acid etching to yield a self-supporting catalyst. The SSM was first applied to M−N−C materials and reported by our group in 2008 and since then has undergone several optimizations.[40−42] A significant advantage of SSM-based catalysts is its tunable hierarchical pore structure, producing a significant

https://doi.org/10.1021/acscatal.4c02717
ACS Catal. 2024, 14, 9797−9811

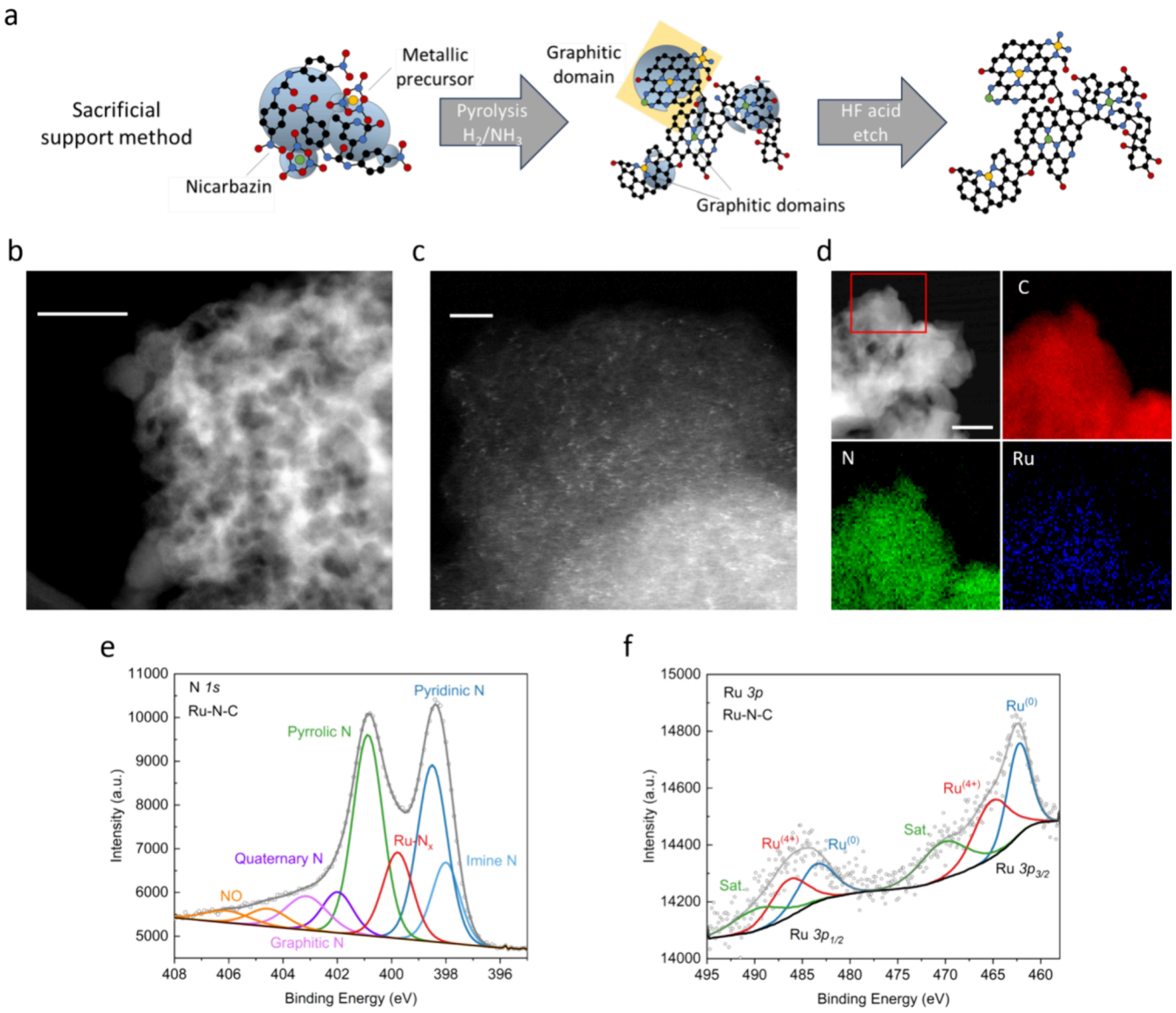

Figure 2. Synthesis approach and characterization for an M−N−C catalyst. (a) Synthesis schematic for the sacrificial support method (SSM), employing nanoporous silica as a sacrificial template. Characterization for Ru−N−C, representative for the set of M−N−C catalysts synthesized by the SSM. Atomic-resolution HAADF-STEM images at (b) low magnification (scale bar is 50 nm), showing the hierarchical porous structure characteristic of SSM catalysts, and (c) high magnification (scale bar is 2 nm), where the bright spots are atomically dispersed Ru−N_x sites. (d) EDS mapping (scale bar is 50 nm) showing the distribution of C, N, and Ru. (e) N 1s XPS spectra, confirming the formation of the Ru−N_x moiety. (f) Ru 3p XPS spectra.

portion of the active M−N_x sites in its mesoporous volume, generating highly reactant accessible sites, in both the gas and liquid phase.[43,44] The general SSM synthesis procedure is shown in Figure 2a, where a metal salt precursor is mixed with a carbon−nitrogen-containing precursor (nicarbazin) and a variety of nanoporous silica. The nicarbazin carbon−nitrogen precursor is selected due to its low melting point, enabling it to melt into the porous structure of the silica prior to decomposition (observed by in situ scanning transmission electron microscopy, STEM) imparting the SSM's characteristic hierarchical pore structure with a leading mesoporosity, as recently visualized via several in situ and operando technqiues.[45,46] After mechanical mixing, the catalyst is pyrolyzed under a reductive atmosphere. This is followed by concentrated hydrofluoric acid etching, removing the template and any metallic nanoparticles, after which an M−N−C catalyst with atomically dispersed M−N_x sites can be obtained. It is important to note that with the SSM, due to the uncontrolled nature of pyrolysis, a variety of M−N_x−C_y and metal-free N−C moieties are formed, not only the idealized M−N_4 site, each with a unique reactivity. Figure 2 shows representative characterizations for the M−N−C catalysts examined in this work, employing Ru−N−C as an example, where the aberration-corrected (AC)-STEM at low magnification in Figure 2b shows the absence of Ru nanoparticles and the hierarchal porous structure characteristic of SSM-based catalysts. The high magnification AC-STEM image in Figure 2c shows the atomically dispersed Ru−N_x sites. The energy dispersive X-ray spectroscopy (EDS) in Figure 2d shows the homogeneous distribution of C, N, and Ru throughout the Ru−N−C catalyst. X-ray photoelectron spectroscopy (XPS) was used to examine the N-moieties and confirm the formation

https://doi.org/10.1021/acscatal.4c02717
ACS Catal. 2024, 14, 9797−9811

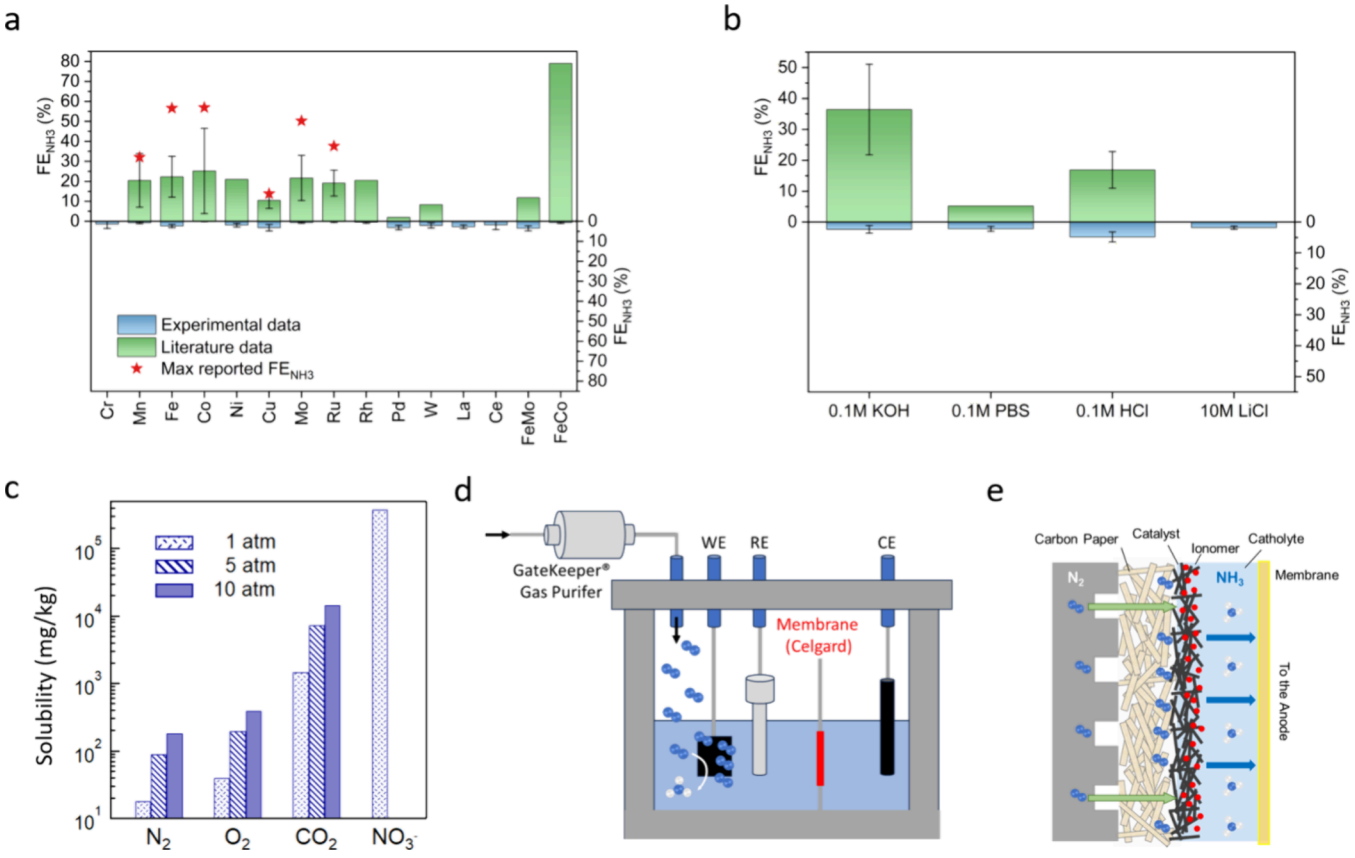

Figure 3. Electrochemical N_2RR experimental and literature evaluation, with outlooks on system level improvements for increased N_2 activation. (a) Comparison of literature results (top, in green) and experimental results under rigorous testing (bottom, in blue) for the N_2RR. (b) Further compasrion of Fe−N−C in acidic, neutral, alkaline, and HER suppressed media. (c) Solubility of common electrochemically reduced molecules as a function of pressure. (d) Example schematic of a pressurized electrochemical two-compartment cell. (e) Example schematic of a flow cell with a gas diffusion electrode.

of the Ru−N_x moiety as shown in the N 1s spectra (Figure 2e). The Ru 3p spectra in Figure 2f show a mixed Ru oxidation state of Ru^0 and Ru^{4+}. The atomically dispersed nature of the M−N−C catalysts has been rigorously characterized by synchrotron-based X-ray absorption spectroscopy (XAS), atomic resolution electron energy loss spectroscopy (EELS), and other techniques as demonstrated in our recent work.[39] High- and low-magnification STEM images showing the hierarchical pore structure and atomically dispersed Fe−N_x and Co−N_x sites of the bimetallic FeCo−N−C catalyst is shown in Figure S1a−c. Figure S1d shows representative X-ray diffraction (XRD) for the FeCo−N−C catalyst, showing the absence of any metallic phases.

NITROGEN REDUCTION REACTION

The N_2RR is the ultimate goal of electrochemical nitrogen transformations to NH_3 as it could enable the carbon-neutral production of NH_3 (or urea if coreduced with CO/CO_2) from nitrogen in the air and water at ambient conditions. Unfortunately, despite the thousands of N_2RR papers in the literature, there remain no rigorous and (independently) reproducible N_2RR studies in aqueous protic electrolytes. The challenges of N_2 activation include the severe difficulty in the selective activation of N_2 over H^+, for the parasitic hydrogen evolution reaction (HER). Ultralow solubility of N_2, inhibiting the dissolved N_2 from reaching the surface of the active site, resulting in low NH_3 partial current densities (j_{NH3}) and extremely small amount of NH_3 produced. Combine these challenges with the ubiquitous NH_3 (or NO_x species) contamination present in N_2RR systems (present in the lab equipment, feed gases, chemicals, and in the catalyst itself), results in the field direct N_2RR remaining in an ambiguous state.[10,13,14]

Interestingly, despite the significant challenges in the selective activation of N_2 over H^+, electrocatalysts comprising most of the periodic table have been reported to be successful for the activation of N_2 (Figure S2). Similarly, for M−N−C catalysts, a variety of M−N_x metal centers, both mono- and bimetallic, have been claimed as successful for achieving selective N_2 activation to NH_3 and in some cases extremely active, achieving a Faradaic efficiency for NH_3 (FE_{NH3}) above 75% (Figure 3a). References for each of the catalysts reported in the top of Figure 3a and Figure 3b are provided in Table S1. The top half of Figure 3a shows N_2RR results for M−N−C catalysts with a variety of M−N_x metal centers as reported in the literature, with error bars included when multiple studies are reported for the same M−N−C and a red star indicating the maximum reported FE_{NH3}. From the literature results, it is apparent that when multiple studies have been reported for a M−N−C, the range of reported FE_{NH3} is extremely wide; for Fe−N−C, as an example, the maximum reported FE_{NH3} is 56%, while other groups report no activity. This extreme discrepancy highlights the ambiguity in the field of the N_2RR.

https://doi.org/10.1021/acscatal.4c02717
ACS Catal. 2024, 14, 9797−9811

To combat this ambiguity and rigorously evaluate the N_2RR activity of M−N−C catalysts, we have recently synthesized a series of 13 atomically dispersed M−N−C catalysts, both mono- and bimetallic, containing 3d, 4d, 5d, and f metal centers all synthesized following the SSM, for the NO_x reduction reactions.[34,39] Additionally, we have recently reported the success of a bimetallic FeMo−N−C catalyst in employing a highly efficiency catalytic cascade mechanism for the NO_3RR.[34] Here, we apply this same set of 13 M−N−C catalysts, covering 3d, 4d, 5d, and f metals, with two bimetallic FeMo− and FeCo−N−C catalysts, to evaluate their ability for N_2 activation for the N_2RR reaction. A rigorous N_2RR testing system was developed as shown schematically in Figure S3a, and the laboratory system in shown in Figure S3b. In addition to research-grade feed gases, a commercial gas purifier (GateKeeper) was implemented to reduce contaminants of interest (NH_3 and NO_x species) down to the parts per trillion level (as noted by the manufacturer). A small-volume custom H-cell was implemented to concentrate any generated NH_3 to be detected and quantified more accurately. A Celgard 3401 porous polypropylene membrane was used to ensure the membrane did not act as either a source or sink for NH_3.[16,47] The developed N_2RR system allowed for the use of $^{14}N_2$ and Ar in a direct gas purge mode, while for isotopically labeled $^{15}N_2$, the system could be operated in a gas circulation mode for a cost-efficient, multipoint, time course electrolysis if positive results were observed using $^{14}N_2$. We implemented a critically important working electrode soaking step prior to the N_2RR experiments, where after the working electrode has been fully prepared (and dried), the working electrode is soaked in the cell at open circuit voltage (OCV) and then the NH_3 level is quantified by UV−vis. This value is employed as the baseline, to prevent any false positives from possible NH_3/NO_x contaminations from the ink/electrode preparation. Linear sweep voltammetry from 0.3 to −0.8 V vs. RHE, covering the potentials examined for the N_2RR is given for each catalyst in Figure S4. Each catalyst was tested at a potential of both −0.20 V and −0.40 V vs. RHE in a 0.1 M KOH electrolyte, a common condition among the N_2RR literature. The experimental results at −0.40 V for each of the M−N−Cs are shown in the bottom half of Figure 3a, where in sharp contrast to the reported literature, it is readily observed that regardless of the metal center of the M−N−C, mono- or bimetallic, no N_2RR activity is observed, showing a maximum FE_{NH3} of less than 5%. Furthermore, in the cases where a nonzero FE_{NH3} is observed, the total charge is extremely small; therefore, a detected NH_3 concentration of ca. 10 ppb (at the limit of detection for UV−vis) yields an unreliable nonzero FE_{NH3}. Since Fe−N−C is the most reported M−N−C for N_2RR, a variety of electrolyte conditions were explored comprising alkaline (0.1 M KOH), neutral (0.1 M PBS), acidic (0.1 M HCl), and a solvating condition (10 M LiCl), reported to suppress the HER, as shown in Figure 3b. From these results, it is again observed that regardless of the electrolyte condition, when tested rigorously, no N_2 activation is observed. Note all chronoamperometry and NH_3 UV-detection curves are at −0.2 and −0.4 V vs. RHE and are given in Figure S5−S14. Therefore, despite the reported literature, we conclude that when tested rigorously, atomically dispersed M−N−Cs do not show direct N_2 activation in protic aqueous electrolytes in an H-cell configuration. In contrast, as will be shown later, all 14 of these M−N−C catalysts demonstrate the successful activation of NO_x species, achieving FE_{NH3} values of up to 100%.

It is important to note that M−N−C catalysts might be active toward the direct N_2RR, however, the commonly employed H-Cell configuration is not adequate. Since the solubility of N_2 in aqueous protic electrolytes is extremely low, as shown in Figure 3c, it is orders of magnitude below that of CO_2 (in which the CO_2RR is known to suffer from solubility/transport issues). Due to the ultralow solubility, in an H-cell configuration, it is difficult to get the N_2 molecule to the surface of the active site to give activation a chance to occur, while being out-competed by H^+. Figures 3d and 3e show possible alternative N_2RR system configurations that both aim to increase the presence of N_2 at the surface of the catalyst. In Figure 3d, a pressurized system is shown schematically where the partial pressure of N_2 can be increased. A pressurized system for the N_2RR was evaluated by Duan et al.,[48] showing promising results. Importantly, as the partial pressure of N_2 is increased in the system, it is even more essential to quantitatively remove any feed gas contaminants, which could increase proportionally to the N_2 partial pressure. Figure 3e schematically shows the use of a GDE, which is commonly employed in CO_2RR systems. The GDE creates a triple phase boundary where the gas-phase N_2 is in direct contact with the solid-phase catalyst and liquid-phase electrolyte. In the GDE configuration, the direct contact of the N_2 with the catalyst presents an opportunity for N_2 activation, while reducing competition from the HER. As the necessity to explore more complex N_2RR systems with favorable N_2 accessibility increases, researchers must keep in mind that the care required to eliminate all possible contamination in these complex systems increases proportionally.[49]

We would like to suggest to the nitrogen reduction community that to make reliable progress in this field, it is not appropriate to selectively choose and satisfy a rigorosity check from one of the many N_2RR protocol papers in the literature to get a manuscript to publication. An alternative methodology is to approach the N_2RR doing everything possible to not find NH_3. After exhausting all means of eliminating NH_3, if NH_3 still remains and is produced in a non-negligible quantity and verified by a multipoint isotopic analysis, the electrocatalyst should then be independently evaluated. If confirmed to a reasonable degree by independent parties, the results should be communicated to the field. Furthermore, such a catalyst should be made available for other groups (such that synthesis uncertainties are eliminated) for evaluation on their own N_2RR systems to obtain much needed activity benchmarks. Unfortunately, without open collaboration between groups and without the development of reliable N_2RR activity benchmarks, progress in the direct N_2RR will remain ambiguous.

NITRATE/NITRITE REDUCTION REACTION

Due to the limited progress made in the N_2RR, several alternative pathways for NH_3 synthesis are being investigated, which led to the resurgence of interest toward the reduction of more oxidized nitrogen species, most notably nitrate (NO_3^-) and nitrite (NO_2^-).[19,50] Although these nitrogens are in a 5^+ and 3^+ oxidation state, respectively, and require either $8e^-$ or $6e^-$ per NH_3 molecule (as opposed to $3e^-$ for N_2), there are a number of advantages to the NO_3^- and NO_2^- reduction reactions (NO_3RR, NO_2RR). In direct opposition to N_2, both NO_3^-/NO_2^- are extremely soluble in aqueous electrolytes at

https://doi.org/10.1021/acscatal.4c02717
ACS Catal. 2024, 14, 9797−9811

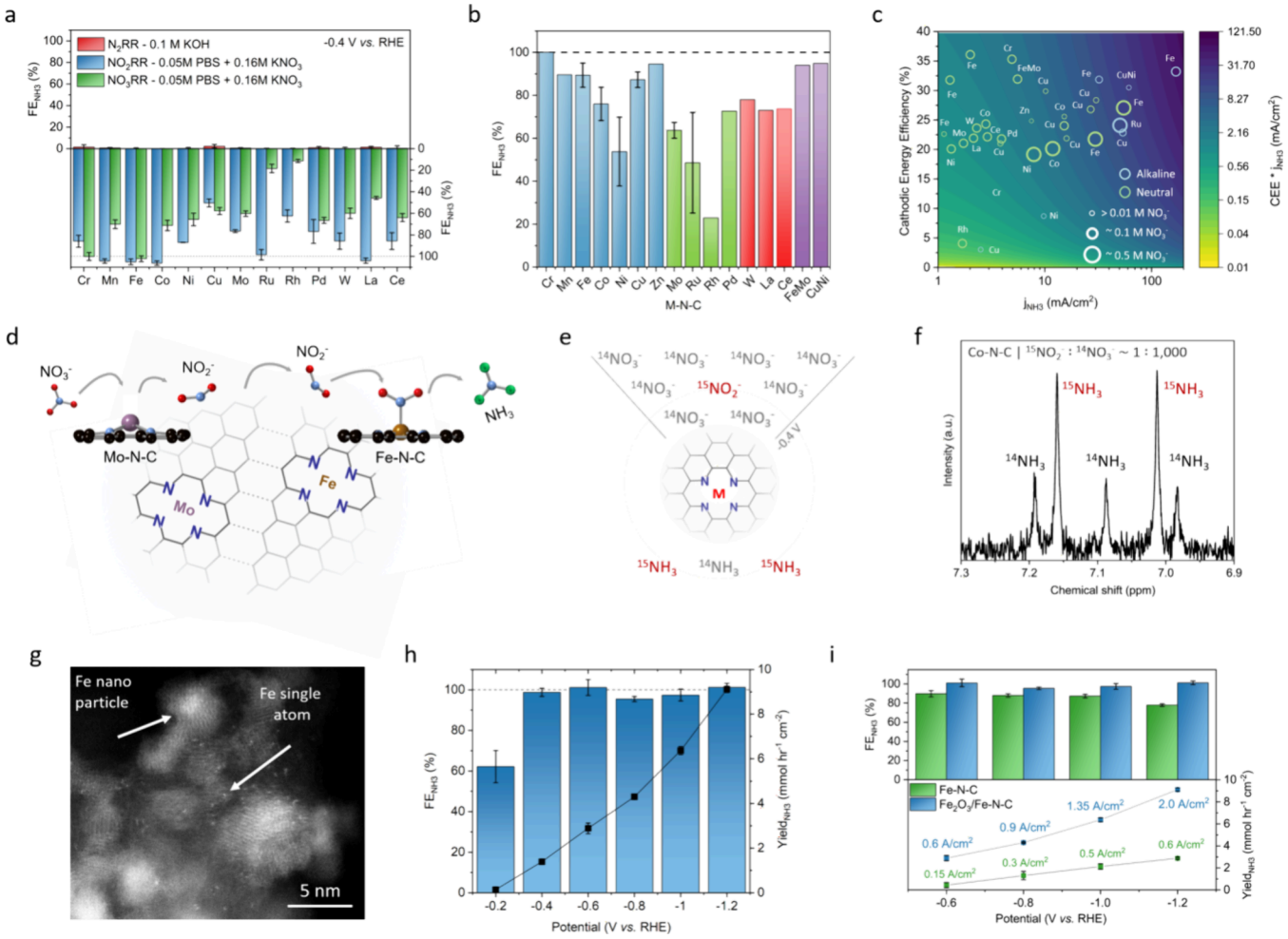

Figure 4. Experimental evaluation of N_2 and NO_3^-/NO_2^- reduction reaction activity over M−N−C catalysts and literature evaluation of M−N−C catalysts for NO_3RR activity. (a) Experimental results comparing N_2 activation and NO_3^-/NO_2^- activation for NH_3 synthesis over M−N−C catalysts in an H-cell system. NO_3RR data adapted with permission, Nature portfolio under CC-BY 4.0 (http://creativecommons.org/licenses/by/4.0/).[39] (b) Literature results for NO_3RR to NH_3 over M−N−C catalysts (mono- and bimetallic). (c) Contour plots comparing the cathodic energy efficiency and NH_3 partial current density for several literature reports, where the color of the circle indicates the pH of the electrolyte (neutral or alkaline) and the size of the circle corresponds to the concentration of NO_3^- used in the study (a larger version is given in Figure S15 for clarity). (d) Proposed cascade mechanism over a bimetallic M−N−C for NO_3^- to NH_3. (e) Isotopic NO_2^- doping to demonstrate the active role of the NO_2^- intermediate and (f) ^{1}H NMR spectra for Co−N−C after NO_3RR electrolysis with isotopically doped $^{15}NO_2^-$. Figures e−f are adapted and reproduced with permission, Nature portfolio under CC-BY 4.0 (http://creativecommons.org/licenses/by/4.0/).[39] (g) AC-HAADF-STEM image of the Fe_2O_3/Fe−N−C. (h) NO_3RR performance using Fe−N−C as a support in the Fe_2O_3/Fe−N−C system (1 M KOH + 0.16 M KNO_3). (i) Comparison of the NO_3RR performance over Fe−N−C as a primary catalyst and Fe_2O_3/Fe−N−C, where Fe−N−C is an active support. Figures g−i are adapted and reproduced with permission, copyright 2024, Wiley-VCH GmbH.[35]

ambient conditions, as shown in Figure 3c, being 5 orders of magnitude greater than N_2. Additionally, it was shown computationally that over atomically dispersed M−N_x sites, NO_3^- has favorable adsorption energies over H^+.[51,52] Increased solubility and favorable adsorption energies readily enable the NO_3^- molecule to selectively reach the active site of the catalyst, leading to the high FE_{NH3} and NH_3 yield rates (Y_{NH3}) reported in the literature (Table S2). Furthermore, the atomically dispersed nature of the M−N_x active sites preferentially inhibits N−N coupling, allowing the selective production of mononitrogen products (e.g., NH_3). Nitrates are an environmental pollutant and are present in industrial waste streams and agricultural water runoffs due to over fertilization practices, enabling the NO_3RR to convert an environmental pollutant into a value-added product. Recent work has demonstrated air stripping and acid trap approaches to concentrate out the produced NH_3 for use.[53] However, the NO_3^- molecule in these wastewater runoffs originates from an NH_3 molecule produced by the HB process; therefore, the NO_3RR is not decoupled entirely from the HB process but enables a more efficient nitrogen cycle. Alternatively, non-thermal (or low-temperature) plasma oxidation processes beginning with N_2, creating, and then reducing NO_3^- to NH_3, offer decoupled carbon-neutral pathways for NH_3 synthesis that leverage the advantages of the high FE_{NH3} and Y_{NH3} of the NO_3RR and are currently comparable in energy efficiency to lithium-mediated N_2RR processes, with reports claiming between 200−400 kWh/kg_{NH3} for both approaches.[54−59]

The NO_3RR/NO_2RR has been explored for a variety of atomically dispersed mono- and bimetallic M−N−Cs with variety of 3d, 4d, 5d, and f metal centers, as shown in Figure 4a and 4b.[30,31,34,39,60] Figure 4a shows the N_2RR, NO_2RR, and NO_3RR performance of the M−N−C catalysts examined in

https://doi.org/10.1021/acscatal.4c02717
ACS Catal. 2024, 14, 9797−9811

Figure 3a, which compares the N_2RR results in this work with the NO_2/NO_3RR results from our recent work.[34,39] It is readily observed that while no N_2RR activity is seen over the series of M−N−Cs, all the M−N−Cs are active for the NO_3RR and generally more active for the NO_2RR. The NO_2RR often shows higher FE_{NH3} and Y_{NH3} than the NO_3RR due to the transformation of NO_3^- to NO_2^- often being regarded as a rate-limiting step in the NO_3RR. Starting with NO_2^- requires only $6e^-$ per NH_3 molecule, and has a reduced standard reduction potential compared to NO_3^-, with relatively small energy barriers for subsequent proton electron transfers.[13] Additionally, it was shown experimentally that even metal-free N−C catalysts are also active for the NO_2/NO_3RR and computationally that the pyridinic, pyrrolic, and graphitic N-moieties all show favorable Gibbs free energies for NO_3^- transformations.[39] These results emphasize that extreme care must be taken in N_2RR experiments to remove any NO_x species as these will readily and selectively be reduced over a variety of M−N_x (and N−C) sites to NH_3. There now exists around a dozen experimental studies (and growing) in the literature that examine the activity of M−N−C catalysts for the NO_3RR and are summarized in Figure 4b, where the FE_{NH3} is examined against the metal center of the M−N−C.[34,39,60−64] Error bars are provided when multiple studies have been reported for the same metal center. From Figure 4b, 3d metals appear to be the most selective for NH_3 synthesis, where Cr−, Mn−, Fe−, Cu−, and Zn−N−C can achieve a FE_{NH3} of ca. 90%, with Cr−N−C and Fe−N−C (in several studies) reaching a FE_{NH3} of 100%. In general, the 4d, 5d, and f-metals display moderate NH_3 selectivity, with a FE_{NH3} of ca. 60%. However, the Ru− and Rh−N−C catalysts display much lower selectivity to NH_3. At mildly reductive potentials, a high selectivity to NH_3 can be achieved (especially in the presence of NO_2^-); however, as a more reductive potential is applied, the HER dominates. Both studies employing bimetallic catalysts show almost 100% FE_{NH3}, due to the reported synergistic effects that enable a cascade catalysis pathway.[34,64] In the N_2RR, the challenge is demonstrating the N_2 activation is even occurring, while for the NO_3/NO_2RR, within a few years, a FE_{NH3} of ca. 100% is appearing almost regularly in the literature. The challenge with the NO_3/NO_2RR is simultaneously achieving high FE_{NH3} and Y_{NH3} at the highest energy efficiency possible. The most common condition for achieving a high Y_{NH3} is a highly alkaline environment (pH 13/14), where the standard reduction potential for NO_3^- to NH_3 is 0.69 V vs. RHE (pH 14).[65] Generally, to achieve a high Y_{NH3} (mmol hr^{-1} cm^{-2}), a potential more reductive than −0.5 V vs. RHE is required, resulting in a cathodic energy efficiency (CEE) of less than ca. 25%. In the field of the NO_3/NO_2RR, comparing catalysts based on either FE_{NH3} and Y_{NH3} is not as meaningful as in the N_2RR, as many catalysts can achieve either high FE_{NH3} with low Y_{NH3} or high Y_{NH3} with reduced FE_{NH3}. A useful comparison is shown in Figure 4c, comparing the CEE against the NH_3 partial current density (j_{NH3}) as shown in a recent work,[35,66] where the CEE incorporates the applied reductive potential and FE_{NH3}, while the j_{NH3} incorporates the Y_{NH3} and FE_{NH3}. In this way, the overall performance of catalysts can be readily compared, with performance increasing toward the top right in Figure 4c, simultaneously achieving increased CEE and j_{NH3}. An additional factor incorporated into this plot is the concentration of NO_3^- in the feed, where larger circles represent higher concentrations of NO_3^-, which generally lead to better performances. From Figure 4c, the highest performing catalyst is Fe−N−C in an alkaline condition, achieving a CEE of 33% at a j_{NH3} of ca. 200 mA/cm^2, while most of the catalysts display a similar, lower CEE (20−25%), however with a wide range of j_{NH3} between 1−70 mA/cm^2, highlighting the utility of Figure 4c over a simple FE_{NH3} comparison (Figure 4b). A complete summary with references for the data points used in Figure 4b and 4c is given in Table S2. A larger version of this Figure is given in Figure S15 for clarity.

BIMETALLIC CATALYSTS

Atomically dispersed bimetallic catalysts present unique advantages for the NO_3RR and enable cascade pathways which can reduce the required overpotential for the reaction, increasing energy efficiency. Bimetallic catalysts can be either two independent M−N_x sites (M_1−N_x and M_2−N_x) or a diatomic M_1M_2−N_x site, in theory. However, to date, the selective synthesis of diatomic sites with statistical relevance is still lacking in the literature. Interestingly, due to the desorbable intermediate NO_2^- in the NO_3RR, a diatomic site is not required in the bimetallic M−N−C. Figure 4d illustrates the NO_3RR cascade catalysis pathway, which takes advantage of the desorbable NO_2^- intermediate.[34] To enable the cascade pathway, it is imperative that the M_1−N_x site selectively reduces NO_3^- to NO_2^-, while the M_2−N_x site is highly active for the $6e^-$ reduction of NO_2^-. Figure 4d gives the example of FeMo−N−C reported in the literature, which leverages the chemical dissociation of NO_3^- to NO_2^- over the Mo−N_4 site, while the Fe−N_4 demonstrated a 100% FE_{NH3} for the reduction of NO_2^- to NH_3, giving an overall FE_{NH3} of 94% for the NO_3RR.[34] Similarly, a CuNi−N−C catalyst was recently reported in the literature, also achieving a high FE_{NH3} above 95%.[64]

It was shown through isotopic $^{15}NO_2^-$ doping experiments, Figure 4e, that even at very low concentrations (1,000 ppm $^{14}NO_3^-$:1 ppm $^{15}NO_2^-$), the NO_2^- in the bulk can readily (re)adsorb over all the M−N−Cs examined in Figure 4a and metal-free N−C catalysts, yielding $^{15}NH_3$.[39] Interestingly, over the Co−N_x sites, $^{15}NO_2^-$, even at low concentrations, yielded more isotopic $^{15}NH_3$ than standard $^{14}NH_3$, revealing the extreme selectivity of NO_2^- over Co−N_x sites (Figure 4f). This demonstrates the opportunities to create highly energy efficient and selective cascade pathways, where an M−N_x site active for NO_3^- to NO_2^- generation could be paired with Co−N_x to achieve the NO_3RR closer to the standard reduction potential.

M−N−Cs AS ACTIVE SUPPORTS

It was recently shown for the ORR that M−N−Cs can serve not only as the primary catalyst, but also as active supports for Pt nanoparticles.[37,38,67,68] The Pt/M−N−C systems have shown increased ORR performance and durability through electronic particle−support and ionomer−support interactions. It is thought that the Pt nanoparticles can draw electrons from the M−N_x sites, creating more favorable intermediate adsorption energies and increasing the anchoring of the Pt nanoparticles. This nanoparticle/M−N−C system was recently demonstrated for the NO_3RR, where sub 5 nm Fe_2O_3 nanoparticles were supported on an atomically dispersed Fe−N−C support.[35] Figure 4g shows a HAADF-STEM image of the Fe_2O_3/Fe−N−C catalyst, where the atomically dispersed Fe sites are observed simultaneously with the Fe_2O_3 particles. The Fe_2O_3/Fe−N−C system enhances the

https://doi.org/10.1021/acscatal.4c02717
ACS Catal. 2024, 14, 9797−9811

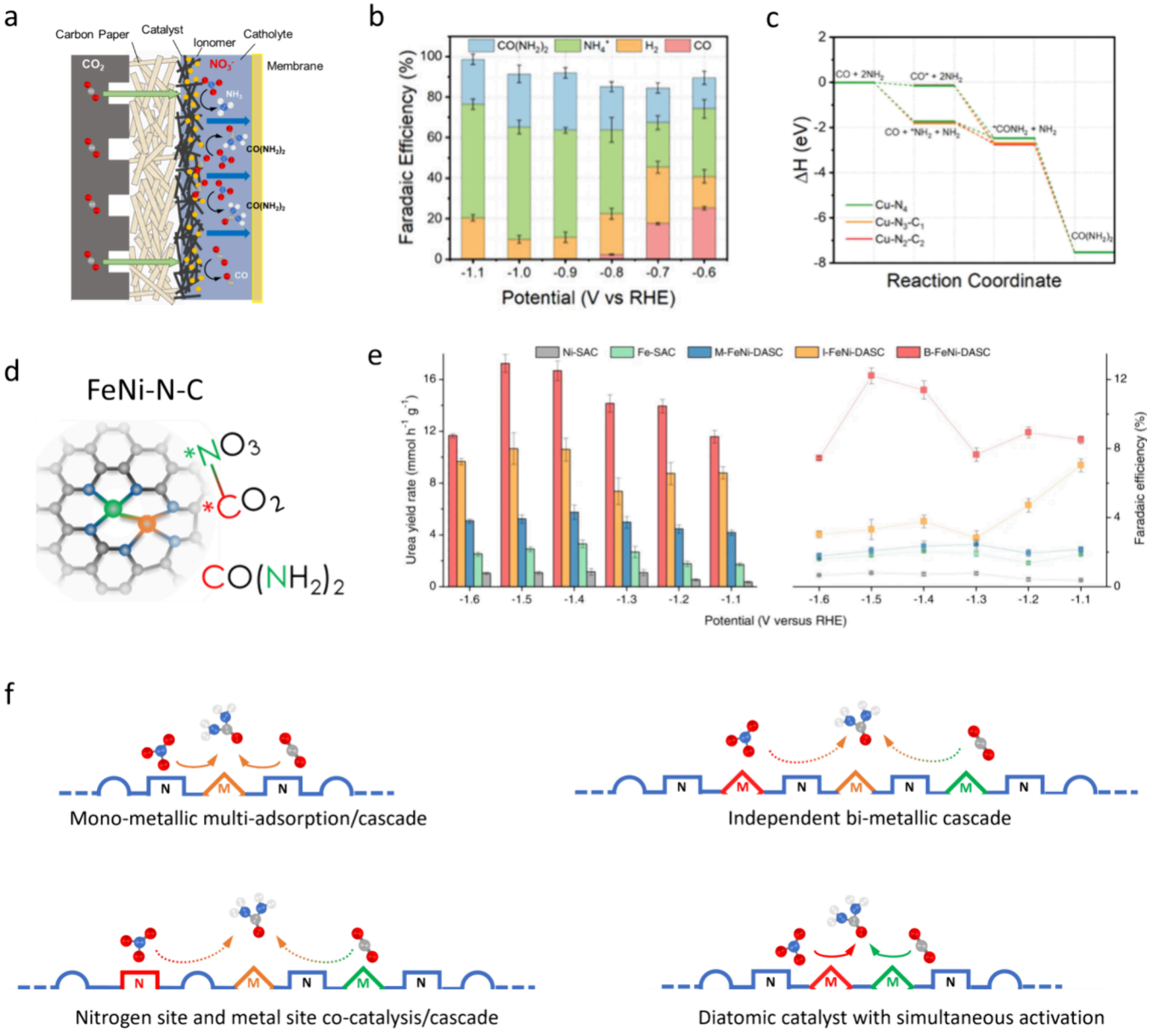

Figure 5. Coupling CO_2 reduction and NO_3^- reduction for C−N bond formation. (a) Schematic for a C−N bond formation using a gas diffusion electrode. (b) Selectivity for urea, NH_3, CO, and H_2 over a Cu−N−C catalyst. (c) Proposed pathway for C−N bond formation over different Cu−N_x−C_y sites. Figures b−c are reproduced with permission, copyright 2022, Wiley-VCH GmbH.[78] (d) Schematic of a diatomic FeNi−N_6 site for simultaneous activation of NO_3^- and CO_2. (e) Yield rate and selectivity for urea syntehsis as a function of potential over an Fe−, Ni−, isolated FeNi−N−C, and diatomic FeNi−N−C catalysts, reproduced with permission, Nature portfolio under CC-BY 4.0 (http://creativecommons.org/licenses/by/4.0/).[32] (f) Proposed pathways for C−N bond formation over atomically dispersed catalyst active sites. Orange arrows or active sites indicate that C−N coupling occurs over a single active site. Red colored arrows or active sites indicate that the NO_3^- activation occurs over this site. Green arrows or active sites indicate that CO_2 activation occurs over these sites. Dashed arrows indicate a reaction pathway with a stable desorbable intermediate, where the reaction occurs in a cascade fashion.

NO_3RR activity in two ways. First, possible electron donation from the Fe−N_x sites to the Fe_2O_3, altering the electronic state of the Fe_2O_3 particles, as the Fe_2O_3 is in the Fe^{3+} state and the Fe−N−C is in a ca. $Fe^{2.5+}$, creating more favorable adsorption energies. Second, by utilizing both Fe_2O_3 and Fe−N−C, a plurality of highly active sites are available for the NO_3RR, greater than solely Fe_2O_3 on a carbon black support or Fe−N−C. Figure 4h shows the performance of the Fe_2O_3/Fe−N−C catalyst in a highly alkaline 1 M KOH + 0.16 M KNO_3 system. Uniquely, the system shows potential independent behavior. At a reductive potential of −0.4 V vs. RHE or greater (more cathodic), a FE_{NH3} of ∼100% is maintained, while increasing the Y_{NH3}. This potential-independent behavior allows the Fe_2O_3/Fe−N−C system to achieve a huge Y_{NH3} of over 9 mmol hr^{-1} cm^{-2} at a FE_{NH3} of 100%, suppressing the HER at highly cathodic potentials, out-competing almost all current reported literature.[69,70] Figure 4i shows that although Fe−N−C suffers from the HER at more cathodic potentials, the Fe_2O_3/Fe−N−C system maintains a 100% FE_{NH3}. This work demonstrates the effectiveness of nanoparticle/M−N−C systems in achieving an ultrahigh partial current density for NH_3. Although the potential limiting behavior enables high j_{NH3} at FE_{NH3} of 100%, the limiting factor of this Fe_2O_3/Fe−N−C system is the large overpotential required, resulting in

https://doi.org/10.1021/acscatal.4c02717
ACS Catal. 2024, 14, 9797−9811

reduced cathodic energy efficiencies (between 20−30%).[35] Future work could achieve a system with high j_{NH3} at higher energy efficiencies by integrating the cascade catalysis approach with a nanoparticle/M−N−C system.

■ ELECTROCHEMICAL C−N BOND FORMATION

Although the typical goal of electrochemical nitrogen transformations is to produce NH_3, largely aimed at the production of synthetic fertilizers, NH_3 is not the final product and needs to undergo a second thermal, energy-intensive reaction with CO_2 to produce urea ($CO(NH_2)_2$). Approximately 70% of NH_3 is utilized to produce urea-based fertilizers.[71] Therefore, it is thought that by electrochemically coreacting CO_2/CO and a reactive nitrogen source, C−N bonds could be formed, yielding a single-step reaction for the carbon-neutral synthesis of urea (fertilizer). There have been reports claiming the successful coactivation of CO_2 and N_2; however, the same challenges that were discussed for the N_2RR are relevant in the coreduction of CO_2 and N_2, resulting in a significant portion of current electrochemical C−N bond formation studies being largely nonrigorous or nonreproducible. Alternatively, the coactivation of CO_2/CO and NO_3^- (or NO_2^-) has been successfully reported several times over the past few years, with relatively high Faradaic efficiency for urea (FE_{urea}), ca. 40% being achieved.[20,72−75] While the coreduction of CO_2 and NO_3^- is a complex multistep $16e^-$, $18H^+$ transfer reaction, this system synergizes perfectly with a flow cell configuration, typically employed for the CO_2RR. Gas-phase CO_2/CO can be supplied through GDE and meet the highly soluble NO_3^-/NO_2^- at the solid surface of the catalyst, creating a triple phase boundary where coactivation can occur, as shown schematically in Figure 5a. Although a flow cell configuration for C−N bond formation over a M−N−C catalyst is yet to be reported, its superior performance over an H-cell configuration has been reported for extended metal surfaces.[20]

To avoid the publication of false positives due to nonrigorous product detection, something that has convoluted the N_2RR with NH_3 quantification, the field of N_2/NO_x and CO_x coactivation must implement rigorous standards now, at the onset of the field. For C−N bond formation, urea is often quantified using simple UV-based methods either through the urease method, during which urea is hydrolyzed into CO_2 and two NH_3 molecules, which are then detected, or through the diacetyl monoxime−thiosemicarbazide (DAMO-TSC) method, which reacts urea and diacetyl monoxime in an acidic media, where the final product can be detected spectroscopically around 520−530 nm. Yet, these common methods are subject to strong interference from NO_xRR byproducts NH_3 and NO_2^-, respectively, which can lead to either false positive or significantly overestimated results.[76] It was recently shown that with the DAMO-TSC method, low concentrations of NO_2^- (a common side product of NO_3RR) had a significant impact on the false positive detection of urea, especially at low urea concentrations, less than 2 ppm, a concentration in which the vast majority of the current reported literature falls, while at 40 ppm of NO_2^-, the DAMO method could overestimate the concentration of urea by 100%. Critically, the same article offers a simple solution to eliminate NO_2^- interference with a modified-DAMO-TSC (M-DAMO-TSC) method, introducing a NO_2^--consuming reaction through the addition of a sulfamic acid and hydrochloric acid solution, reducing errors in urea detection to below 5% for up to 50 ppm of NO_2^-.[77] Other methods such as ^{1}H NMR or HPLC could quantify urea as well and could avoid NO_2^- interference; however, these methods have lower accessibility and a higher limit of detection, 5 ppm for ^{1}H NMR (500 MHz, 1000 scans) and 0.5 ppm for HPLC. Given the availability and ease of use for UV-based detection with the DAMO-TSC method, this will likely be the standard for most research. Therefore, given the ease with which the NO_2^- interference could be reduced, it is imperative that researchers employ this M-DAMO-TSC method in instances where the urea produced is below 2 ppm. Ideally, the M-DAMO-TSC method will be used in combination with ^{1}H NMR or HPLC for multimethod confirmation.

To date, the use of atomically dispersed M−N−C catalysts for electrochemical C−N bond formation is extremely limited, with only a handful experimental studies[32,78−81] available in the literature as well as a computational study.[82] It was recently demonstrated that atomically dispersed Cu−N_x sites are active for the coactivation of CO_2 and NO_3^-.[78] The study modified the coordination environment of the Cu−N_x sites by changing the pyrolysis temperature (as observed by XAS). The Cu−N_4 sites showed high CO_2RR activity, while the Cu−N_{4-x}−C_x sites showed favorable NO_3RR activity. When CO_2 and NO_3^- are coreacted over the Cu−N_4 sites, a relatively high FE_{urea} of 28% is achieved at −0.9 V vs. RHE in an H-cell configuration, as shown in Figure 5b. This work uses a 0.1 M K_2SO_4 + 0.1 M KNO_3 electrolyte in an H-cell system, which results in the large concentration of the highly soluble NO_3^- reducing to NH_3, accounting for most of the current. DFT was employed to evaluate the energy barrier for the C−N bond formation step, hypothesized to be between the *CO and *NH_2 intermediates, showing the lowest energy barrier for the C−N bond forming step, over the Cu−N_4 site. This study was the first to successfully employ M−N−C materials for electrochemical C−N bond formation. In contrast to this, a recent study also employing Cu−N−C and N−C reported that the Cu−N_x metal center causes a decrease in the FE_{urea}, reporting a maximum of ca. 15%, due to the preferential reduction of NO_3^- to NH_3 over the Cu−N_x sites. Reporting that the metal-free N−C, particularly the C═N−H moiety, has substantial urea selectivity, with a maximum FE_{urea} greater than 60%. While impressive, it should be noted that the main side product in this work is NO_2^-, known to significantly interfere with the accuracy of the DMAO-TSC method of urea quantification, as discussed previously.[76]

Another recent study reports the use of a diatomic FeNi−N−C catalyst, composed of FeNi−N_6 sites, shown schematically in Figure 5d.[32] The diatomic FeNi−N−C achieves an impressive FE_{urea} of 17.8% at an optimized potential of −0.9 V vs. RHE, with the largest side product again being NH_3, is shown in Figure 5e. Independently, the Fe−N_4 site can achieve a NO_3^- to NH_3 FE_{NH3} of ca. 80%, while the Ni−N_4 site can achieve a CO_2 to CO FE_{CO} of ca. 85%. The authors claim that a diatomic FeNi−N−C catalysts (with a Fe−Ni−N_6) active site is the most active for C−N bond formation, while a bimetallic catalyst with independent Fe−N_4, Ni−N_4 sites and monometallic Fe−N_4 and Ni−N_4 catalyst are also active for urea synthesis, at a lower urea yield rate (Y_{urea}) and FE_{urea}. Again, in this study, urea was quantified by the urease decomposition method and ^{1}H NMR. However, not enough information is given such that their total ppm of urea can be calculated; therefore, it is unclear if these methods were appropriate for accurate urea quantification.

https://doi.org/10.1021/acscatal.4c02717
ACS Catal. 2024, 14, 9797−9811

Interestingly, from these studies, the coreduction of CO_2 and NO_3^- can occur over either individual N−C sites, M−N_x sites, independent M_1−N_x and M_2−N_x sites in a bimetallic catalysts, or over diatomic M_1-M_2−N_x sites, implying that a deep fundamental understanding of this complex reaction is required to guide advanced catalyst/system designs. Figure 5f schematically demonstrates four possible reaction pathways for C−N bond formation over M−N−C catalysts. The first pathway (top left of Figure 5f) presents the case of a monometallic M−N−C, in which the metal center has the ability to simultaneously adsorb both the CO_2 and NO_3^- species to electrochemically form the C−N bond over a single metal center (this could of course be split into a sequential adsorption and activation, e.g., CO_2 to *CO then react with NO_3^-). It was demonstrated in a recent work utilizing a Mo−N−C catalyst for the NO_3RR, that the Mo−N_4 site could simultaneously adsorb two intermediates. Analogously, a metal center with a large coordination number could enable the simultaneous adsorption of C and N species. The second scenario (in the bottom left of Figure 5f) shows reactant species, here NO_3^- being activated by a metal free N-moiety, while the CO_2 is activated by the M−N_x site. The two activations could take place in a very localized proximity, such that a C−N bond could be formed in a cascade fashion over an independent active site (as shown), if the C−N bond pathway allows for stable desorbable/readsorbable intermediates (or locally channeled), as observed in the NO_3RR. The third scenario (top right of Figure 5f) shows a bimetallic catalyst, with independent M_1−N_x and M_2−N_x sites, where each site selectively targets a given reaction, either CO_2 activation or NO_3^- activation. This scenario is difficult to deconvolute as the C−N bond formation occurs either via a cascade pathway between the two independent M−N_x sites, a M−N_x site with a metal-free N-moiety, or with each individual M−N_x site activating both reactants (or even a combination of all of these). The final scenario is the most intuitive (bottom right of Figure 5f), where a diatomic M_1−M_2−N_x site is employed in which one site is tailored to activate CO_2 and the other to activate NO_3^- adjacent to each other, such that a C−N bond can be readily formed. However, in practice, it is extremely difficult to synthesize a diatomic catalyst with a statistically meaningful selectivity for diatomic M_1−M_2−N_x sites (particularly with commonly employed pyrolysis-based methods in which precise control is difficult).

CONCLUSION/OUTLOOK

While significant progress has been made in the materials development of atomically dispersed M−N−C catalysts and their application to electrochemical transformations of reactive nitrogen species, several key challenges must be addressed to further these technologies and move them beyond the laboratory scale. Each reaction (N_2RR, NO_3RR, and C−N bond formation) has its own unique challenges and will each be briefly discussed.

Before discussing the reactions, the M−N−C catalyst development and characterization must be mentioned. To advance the efficacy of M−N−C catalysts for the NO_3RR (and C−N bond formation), the optimization of liquid-phase accessible sites must be improved. This was analogously achieved for gas-phase reactants by employing gas phase transmetalation approaches for Fe−N−C catalyst for the ORR. An inspiring recent work demonstrated that liquid-phase transmetalation is possible (although complex) for an Fe−N−C catalyst.[83] This would allow for maximum site utilization for the NO_3RR. For cascade pathways or C−N bond formation, the popularity of bimetallic catalysts is increasing; however, it is largely unclear if the proposed diatomic sites are being selectively formed, often accompanied by STEM images indiscriminately circling atomically dispersed sites (on a 2D image where sites could be at different Z-heights). There is a need for novel synthesis techniques for selectively synthesizing diatomic sites and to accompany this, a more rigorous evaluation/review when claiming the successful formation of diatomic sites with statistical relevance, especially when forming computational pathways based on these sites.

Of the three reactions examined in this work, the N_2RR faces the largest challenges due to its assumed maturity resulting from the thousands of papers published on the reaction. Despite this, the direct aqueous N_2RR still remains unproven as shown by the rigorous testing in this work over the 15 M−N−C catalysts (mono- and bimetallic) studied and by several other works rigorously evaluating the N_2RR. In order to progress the N_2RR, rather than focus on new catalysts for a nonoptimal H-cell system, new testing configurations need to be explored, such as flow cells with GDE or pressurized systems all focused on increasing the partial pressure of N_2 at the surface of the catalyst. However, in the implementation of these more complex configurations, an extreme level of rigorosity in the electrochemical testing must be maintained. Furthermore, to create confidence in the field of N_2 reduction, any positive results confirmed through multipoint quantitative isotopic analysis should be repeated by an independent group—a.k.a. "beta-testing" for verification (something which to date has not been achieved).

Alternatively, for the NO_3RR, rapid progress has been made, where FE_{NH3} above 90% is widely achieved. Here, the challenge is not in achieving high Y_{NH3} or high FE_{NH3}, but rather achieving them simultaneously and, furthermore, doing so at an overpotential close to its thermodynamic potential. Currently, the cathodic energy efficiency for the NO_3RR is largely below 30%, especially when aimed at Y_{NH3} above several mmol hr^{-1} cm^{-2}. One of the main advantages currently unique to the NO_3RR over other NH_3 synthesis pathways is the ability to achieve extremely high yield rates. To fully utilize this advantage, these high yields must be achieved at moderate energy efficiencies, which makes them more economically competitive. One possible pathway to achieve this is by taking advantage of the cascade pathways enabled by the desorption/readsorption of reaction intermediates to reduce the required overpotential (pulsed potentials could be advantageous in this regard). Future work should focus on translating these high FE_{NH3} and Y_{NH3} to flow cell systems, showcasing the feasibility in scaling these performances, while also exploring the combination of plasma-assisted NO_x generation and NO_xRR systems for NH_3 synthesis totally decoupled from the HB process.

While important initial progress has been made with M−N−C catalysts for C−N bond formation, these works have highlighted the extreme complexity of the reaction and possible reaction pathways. A deeper understanding of how the reaction proceeds over monometallic sites (cascade or dual adsorption), metal-free N−C sites, and diatomic sites will enable the rational development of highly active M−N−C catalysts that can tailor to an optimal reaction pathway. A better mechanistic understanding can also reveal if desorbable/readsorbable (chemically stable) intermediates exist, such that

https://doi.org/10.1021/acscatal.4c02717
ACS Catal. 2024, 14, 9797−9811

cascade pathways are viable. Gaining a deeper understanding will require significant effort combining operando techniques, isotopic doping experiments, and computational studies. Additionally, flow cell systems with GDEs should be implemented to take advantage of the gas-phase CO_2/CO with liquid-phase NO_3^-/NO_2^-, increasing the presence of CO_2/CO at the catalyst surface (to compete with the dominating presence of the extremely high solubility of NO_3^- in H-cell systems). An additional challenge of NH_3 accumulation in the electrolyte must be addressed. An interesting approach could be a second downstream reaction, where CO and NH_3 containing electrolyte are reacted over an extended metal surface to synthesize more complex C−N bond molecules, increasing the overall C−N bond efficiency, as recently demonstrated.[84] As C−N bond formation current densities increase, further challenges with NO_3^-/NO_2^- depletion become relevant. One possible solution is to tailor the electrolyte reservoir size, which could include a constant rate of electrolyte refreshing to maintain an optimal reactant concentration to sustain a high performance. An extreme emphasis on the rigorosity of urea quantification methods must be invoked in the field now, to prevent ambiguity through false positive reports (as has plagued the N_2RR field). At a minimum, researchers are required to utilize the M-DAMO-TSC method for UV-based detection (or robustly verify no influence of NO_2^-). Alternatively, if appropriately high urea concentrations can be verified, then methods such as ^{1}H NMR or HPLC can be used. In the best case, a multimethod detection of urea will be used. Finally, as progress is achieved in the N_2RR in flow cell systems, additional progress can readily be translated to C−N systems to achieve the ultimate goal of utilizing CO_2 and N_2 to create urea in a carbon-neutral fashion. However, extreme caution must be practiced now to ensure the rigorosity of any C−N bond systems employing N_2 as a reactant and to ensure the field does not become flooded with false positives, hindering its progress and validity.

METHODS

Catalyst Synthesis. The library of atomically dispersed M−N−C catalysts both mono- and bimetallic utilized in this work for the N_2RR, were originally synthesized for two NO_3RR studies reported in the literature.[34,39]

Briefly, 6.26 g of Nicarbazin, 1.25 g of OX-50 (silica), 1.25 g of LM-150 (silica), 0.5 g of Stöber spheres, and a metal salt precursor were combined in water under constant stirring. The catalyst mixture was then sonicated for 30 min and then dried at 45 °C overnight under constant stirring. The catalyst slurry was then transferred to an oven at 45 °C for 24 h to ensure complete drying. The catalyst mix was then ball milled at 45 Hz for 1 h and then pyrolyzed in a reductive H_2/Ar atmosphere at 975 °C for 45 min. The pyrolyzed catalyst powder is then ball milled for a second time at 45 Hz for 1 h and then etched in concentrated 18 M HF for 96 h. After filtration and drying, the now pyrolyzed and etched catalyst powder undergoes a second pyrolysis step in a reductive NH_3/N_2 atmosphere at 950 °C for 30 min. The catalyst powder is then ball milled for a third time and is ready for use.

The exact amount of metal salt precursor, pyrolysis conditions, and etching media was optimized for each metal center to ensure the formation of atomically dispersed M−N_x sites.

Physical Characterization. Complete characterization of bimetallic FeMo−N−C and a library of M−N−C catalysts is given in references 34 and 45, respectively, containing XRD, BET, Raman, ICP-MS, SEM, STEM, EDS, XPS, EELS, XANES, and EXAFS.

For the Ru−N−C catalyst, X-ray photoelectron spectroscopy was performed by using a Kratox AXIS Supra spectrometer with a monochromatic Al Kα source (1486.6 eV). A 160 eV pass energy from 1400 to 5 eV with a step size of 1 eV was employed for the survey spectra. Charge neutralization was not employed. To analyze the data, CasaXPS software was used, with the C 1s sp^2 peak (284.8 eV) being used for spectrum calibration. A Shirley background was used for the N 1s spectra with a 70% Gaussian and 30% Lorentzian being applied. The crystal structure was analyzed by XRD on a Rigaku Ultima-III powder X-ray diffractometer. The atomically dispersed sites and pore structure of the catalyst were visualized through aberration-corrected scanning transmission electron microscopy, while the elemental distribution was probed through energy dispersive X-ray spectroscopy on a JEOL ARM300CF at 300 keV accelerating voltage.

Electrochemical Measurements. The N_2RR experiments were perfomed using an AutoLab potentiostat without *iR* correction. Ultrahigh purity N_2 gas (99.9995% Praxair) was purged at 40 sccm throughout the electrochemical experiments. All feed gas passed through a commercial gas purifier GateKeeper to remove all contaminants of interest to the ppt level. A custom two-compartment H-Cell (Adams and Chittenden) was used with a cathodic and anodic chamber volume of 30 mL each. The electrolyte used was 0.1 M KOH (pH 13), a common electrolyte reported for N_2RR experiments. A polypropylene Celgard 3401 membrane was used to prevent the membrane from acting as a source or sink of NH_3. A carbon paper (fuel cell store) working electrode was used with a working area of 1 cm^2 onto which the catalyst ink was drop cast for a loading of 0.5 mg/cm^2. The catalyst ink was prepared using 5 mg of catalyst, 300 μL of water, 580 μL of IPA, and 20 μL of Nafion.

During the electrochemical experiments, the background level of NH_3 in the 0.1 M KOH electrolyte was sampled. Then the working electrode was soaked in the electrolyte for 30 min at OCV, and then the electrolyte was sampled again to account for any NH_3 desorbing from the electrode (this level of detected NH_3 was then used as the background level). Chronoamperometry measurements were performed for 1 h at −0.4 V vs. RHE, and the electrolyte was sampled for NH_3.

Product Detection. NH_3 was detected and quantified using UV−vis on a Shimadzu, UV-2600 system, following the Berthelot reaction. A 2 mL sample was mixed with 2 mL of a 1 M NaOH solution containing 5 wt % sodium citrate and 5 wt % salicylic acid. To this, 1 mL of a 0.05 M NaClO solution and 0.2 mL of a 1 wt % sodium nitroferricyanide solution were added. The mixture was incubated for 1 h in the dark, and the absorbance at 655 nm was recorded. The NH_3 was quantified by comparing the sample absorption at 655 nm to the calibration curve generated utilizing standard reference solutions (Figure S16).

Calculation of the Faradaic Efficiency and Yield Rate. The Faradaic efficiency for NH_3 from N_2 was calculated by using eq 1.

$$FE_{NH3} = \frac{c_{NH3} \times V}{Mw_{NH3} \times t^* A_{we}} \quad (1)$$

The yield rate of NH_3 from N_2 was calculated by using eq 2.

https://doi.org/10.1021/acscatal.4c02717
ACS Catal. 2024, 14, 9797−9811

$$Y_{NH3} = \frac{n \times F \times c_{NH3} \times V}{Mw_{NH3} \times Q} \quad (2)$$

Where C_{NH3} is the concentration of NH_3 in the cathodic chamber (μg/mL), V is volume of the electrolyte in the cathodic chamber (30 mL), Mw_{NH3} is the molar mass of NH_3 (17.031 g/mol), t is the CA duration (hr), A_{we} is the area of the working electrode (1 cm^2), n is the number of electrons transferred per NH_3 molecule (3 for N_2 to NH_3, 6 for NO_2^- to NH_3, and 8 for NO_3^- to NH_3), F is Faradays constant (96,485 C/mol), and Q is the total charge transferred during the electrolysis.

The cathodic energy efficiency is calculated using the following equation:

$$\frac{(1.23 - E^0)}{(1.23 - E)} \times FE_{NH3} \quad (3)$$

Where 1.23 is the standard reduction potential for the oxygen evolution reaction (OER) occurring at the anode. E^0 is the standard reduction potential for the NO_3RR, FE_{NH3} is the Faradaic efficiency for NH_3, and E is the applied potential. This calculation assumes no overpotential at the anode for the OER and is therefore called the cathodic energy efficiency for the NO_3RR.

■ ASSOCIATED CONTENT

Supporting Information

The Supporting Information is available free of charge at https://pubs.acs.org/doi/10.1021/acscatal.4c02717.

Atomic-resolution STEM images and XRD for FeNi−N−C; schematic and image of the N_2RR set up; linear sweep voltammetry for all M−N−C catalysts in 0.1 M KOH electrolyte; N_2RR chronoamperometry at −0.20 and −0.40 V vs. RHE with corresponding UV−vis detection of NH_3 for all M−N−Cs; full-size contour plot of Figure 4c for improved clarity; UV−vis calibration curves; comparison tables for N_2RR and NO_3RR (PDF)

■ AUTHOR INFORMATION

Corresponding Author

Plamen Atanassov − *Department of Chemical and Biomolecular Engineering, National Fuel Cell Research Center, University of California, Irvine, California 92697, United States;* orcid.org/0000-0003-2996-472X; Email: plamen.atanassov@uci.edu

Authors

Eamonn Murphy − *Department of Chemical and Biomolecular Engineering, National Fuel Cell Research Center, University of California, Irvine, California 92697, United States;* orcid.org/0000-0003-4675-0846

Yuanchao Liu − *Department of Chemical and Biomolecular Engineering, National Fuel Cell Research Center, University of California, Irvine, California 92697, United States;* orcid.org/0000-0002-3669-8071

Baiyu Sun − *Department of Chemical and Biomolecular Engineering, National Fuel Cell Research Center, University of California, Irvine, California 92697, United States;* orcid.org/0000-0002-6361-9682

Yu-Han Chen − *Department of Chemical and Biomolecular Engineering, National Fuel Cell Research Center, University of California, Irvine, California 92697, United States*

Shengyuan Guo − *Department of Chemical and Biomolecular Engineering, National Fuel Cell Research Center, University of California, Irvine, California 92697, United States;* orcid.org/0000-0002-3457-9554

Complete contact information is available at: https://pubs.acs.org/10.1021/acscatal.4c02717

Notes

The authors declare no competing financial interest.

■ ACKNOWLEDGMENTS

The authors acknowledge the use of facilities and instrumentation at the UC Irvine Materials Research Institute (IMRI), which is supported in part by the National Science Foundation through the UC Irvine Materials Research Science and Engineering Center (DMR-2011967). This work is supported in part by a subcontract from U.S. Department of Energy (DOE), Office of Energy Efficiency and Renewable Energy (EERE), Bioenergy Technologies Office (DE-EE0008923) led by Colorado State University.

■ REFERENCES

(1) van Geem, K. M.; Galvita, V. V.; Marin, G. B. Making Chemicals with Electricity. *Science (80-.).* **2019**, *364* (6442), 734−735.

(2) Schiffer, Z. J.; Manthiram, K. Electrification and Decarbonization of the Chemical Industry. *Joule* **2017**, *1* (1), 10−14.

(3) Tackett, B. M.; Gomez, E.; Chen, J. G. Net Reduction of CO2 via Its Thermocatalytic and Electrocatalytic Transformation Reactions in Standard and Hybrid Processes. *Nat. Catal.* **2019**, *2* (5), 381−386.

(4) Rabinowitz, J. A.; Kanan, M. W. The Future of Low-Temperature Carbon Dioxide Electrolysis Depends on Solving One Basic Problem. *Nat. Commun.* **2020**, *11* (1), 10−12.

(5) MacFarlane, D. R.; Cherepanov, P. V.; Choi, J.; Suryanto, B. H. R.; Hodgetts, R. Y.; Bakker, J. M.; Ferrero Vallana, F. M.; Simonov, A. N. A Roadmap to the Ammonia Economy. *Joule* **2020**, *4* (6), 1186−1205.

(6) Soloveichik, G. Electrochemical Synthesis of Ammonia as a Potential Alternative to the Haber-Bosch Process. *Nat. Catal.* **2019**, *2* (5), 377−380.

(7) Suryanto, B. H. R.; Du, H. L.; Wang, D.; Chen, J.; Simonov, A. N.; MacFarlane, D. R. Challenges and Prospects in the Catalysis of Electroreduction of Nitrogen to Ammonia. *Nat. Catal.* **2019**, *2* (4), 290−296.

(8) Iriawan, H.; Andersen, S. Z.; Zhang, X.; Comer, B. M.; Barrio, J.; Chen, P.; Medford, A. J.; Stephens, I. E. L.; Chorkendorff, I.; Shao-Horn, Y. Methods for Nitrogen Activation by Reduction and Oxidation. *Nat. Rev. Methods Prim.* **2021**, *1* (1), 56.

(9) Ren, Y.; Yu, C.; Tan, X.; Huang, H.; Wei, Q.; Qiu, J. Strategies to Suppress Hydrogen Evolution for Highly Selective Electrocatalytic Nitrogen Reduction: Challenges and Perspectives. *Energy Environ. Sci.* **2021**, *14* (3), 1176−1193.

(10) Ye, D.; Tsang, S. C. E. Prospects and Challenges of Green Ammonia Synthesis. *Nat. Synth.* **2023**, *2* (7), 612−623.

(11) Han, G. F.; Li, F.; Chen, Z. W.; Coppex, C.; Kim, S. J.; Noh, H. J.; Fu, Z.; Lu, Y.; Singh, C. V.; Siahrostami, S.; Jiang, Q.; Baek, J. B. Mechanochemistry for Ammonia Synthesis under Mild Conditions. *Nat. Nanotechnol.* **2021**, *16* (3), 325−330.

(12) Dong, Q.; Yao, Y.; Cheng, S.; Alexopoulos, K.; Gao, J.; Srinivas, S.; Wang, Y.; Pei, Y.; Zheng, C.; Brozena, A. H.; Zhao, H.; Wang, X.; Toraman, H. E.; Yang, B.; Kevrekidis, I. G.; Ju, Y.; Vlachos, D. G.; Liu, D.; Hu, L. Programmable Heating and Quenching for Efficient Thermochemical Synthesis. *Nature* **2022**, *605* (7910), 470−476.

(13) Choi, J.; Suryanto, B. H. R.; Wang, D.; Du, H. L.; Hodgetts, R. Y.; Ferrero Vallana, F. M.; MacFarlane, D. R.; Simonov, A. N. Identification and Elimination of False Positives in Electrochemical Nitrogen Reduction Studies. *Nat. Commun.* **2020**, *11* (1), 1−10.

(14) Sveinbjörnsson, A.; Gunnarsdóttir, A. B.; Creel, E. B.; Canales, C. P.; Zulevi, B.; Lyu, X.; Jafta, C. J.; Skúlason, E.; Serov, A.; Flosadóttir, H. D. Demonstration of No Catalytical Activity of Fe-N-C and Nb-N-C Electrocatalysts toward Nitrogen Reduction Using In-line Quantification. *SusMat* **2022**, *2* (4), 476−486.
(15) Lazouski, N.; Manthiram, K. Ambient Lithium-Mediated Ammonia Synthesis. *Trends Chem.* **2019**, *1* (1), 141−142.
(16) Andersen, S. Z.; Čolić, V.; Yang, S.; Schwalbe, J. A.; Nielander, A. C.; McEnaney, J. M.; Enemark-Rasmussen, K.; Baker, J. G.; Singh, A. R.; Rohr, B. A.; Statt, M. J.; Blair, S. J.; Mezzavilla, S.; Kibsgaard, J.; Vesborg, P. C. K.; Cargnello, M.; Bent, S. F.; Jaramillo, T. F.; Stephens, I. E. L.; Nørskov, J. K.; Chorkendorff, I. A Rigorous Electrochemical Ammonia Synthesis Protocol with Quantitative Isotope Measurements. *Nature* **2019**, *570* (7762), 504−508.
(17) Du, H. L.; Chatti, M.; Hodgetts, R. Y.; Cherepanov, P. V.; Nguyen, C. K.; Matuszek, K.; MacFarlane, D. R.; Simonov, A. N. Electroreduction of Nitrogen with Almost 100% Current-to-Ammonia Efficiency. *Nature* **2022**, *609* (7928), 722−727.
(18) Duca, M.; Koper, M. T. M. Powering Denitrification: The Perspectives of Electrocatalytic Nitrate Reduction. *Energy Environ. Sci.* **2012**, *5* (12), 9726−9742.
(19) van Langevelde, P. H.; Katsounaros, I.; Koper, M. T. M. Electrocatalytic Nitrate Reduction for Sustainable Ammonia Production. *Joule* **2021**, *5* (2), 290−294.
(20) Tao, Z.; Rooney, C. L.; Liang, Y.; Wang, H. Accessing Organonitrogen Compounds via C-N Coupling in Electrocatalytic CO2Reduction. *J. Am. Chem. Soc.* **2021**, *143* (47), 19630−19642.
(21) Li, J.; Zhang, Y.; Kuruvinashetti, K.; Kornienko, N. Construction of C-N Bonds from Small-Molecule Precursors through Heterogeneous Electrocatalysis. *Nat. Rev. Chem.* **2022**, *6* (5), 303−319.
(22) Jasinski, R. A New Fuel Cell Cathode Catalyst. *Nature* **1964**, *201*, 1212.
(23) Jasinski, R. Cobalt Phthalocyanine as a Fuel Cell Cathode. *J. Electrochem. Soc.* **1965**, *112* (5), 526.
(24) Gupta, S.; Tryk, D.; Bae, I.; Aldred, W.; Yeager, E. Heat-Treated Polyacrylonitrile-Based Catalysts for Oxygen Electroreduction. *J. Appl. Electrochem.* **1989**, *19* (1), 19−27.
(25) Lefèvre, M.; Proietti, E.; Jaouen, F.; Dodelet, J. P. Iron-Based Catalysts with Improved Oxygen Reduction Activity in Polymer Electrolyte Fuel Cells. *Science (80-.).* **2009**, *324* (5923), 71−74.
(26) Asset, T.; Atanassov, P. Iron-Nitrogen-Carbon Catalysts for Proton Exchange Membrane Fuel Cells. *Joule* **2020**, *4* (1), 33−44.
(27) Asset, T.; Maillard, F.; Jaouen, F. Electrocatalysis with single metal atom sites in doped carbon matrices. In *Supported Metal Single Atom Catalysis*, 1st ed.; Serp, P.; Minh, P., Eds.; Wiley-VCH, 2022, Chapter 13, pp 531− 582.
(28) Varela, A. S.; Ju, W.; Bagger, A.; Franco, P.; Rossmeisl, J.; Strasser, P. Electrochemical Reduction of CO2 on Metal-Nitrogen-Doped Carbon Catalysts. *ACS Catal.* **2019**, *9* (8), 7270−7284.
(29) Li, J.; Pršlja, P.; Shinagawa, T.; Martín Fernández, A. J.; Krumeich, F.; Artyushkova, K.; Atanassov, P.; Zitolo, A.; Zhou, Y.; García-Muelas, R.; López, N.; Pérez-Ramírez, J.; Jaouen, F. Volcano Trend in Electrocatalytic Co2 Reduction Activity over Atomically Dispersed Metal Sites on Nitrogen-Doped Carbon. *ACS Catal.* **2019**, *9* (11), 10426−10439.
(30) Wu, Z.; Karamad, M.; Yong, X.; Huang, Q.; Cullen, D. A.; Zhu, P.; Xia, C.; Xiao, Q.; Shakouri, M.; Chen, F.; Kim, J. Y.; Xia, Y.; Heck, K.; Hu, Y.; Wong, M. S.; Li, Q.; Gates, I.; Siahrostami, S.; Wang, H. Electrochemical Ammonia Synthesis via Nitrate Reduction on Fe Single Atom Catalyst. *Nat. Commun.* **2021**, *12* (1), 2870.
(31) Li, P.; Jin, Z.; Fang, Z.; Yu, G. A Single-Site Iron Catalyst with Preoccupied Active Centers That Achieves Selective Ammonia Electrosynthesis from Nitrate. *Energy Environ. Sci.* **2021**, *14* (6), 3522−3531.
(32) Zhang, X.; Zhu, X.; Bo, S.; Chen, C.; Qiu, M.; Wei, X.; He, N.; Xie, C.; Chen, W.; Zheng, J.; Chen, P.; Jiang, S. P.; Li, Y.; Liu, Q.; Wang, S. Identifying and Tailoring C-N Coupling Site for Efficient Urea Synthesis over Diatomic Fe-Ni Catalyst. *Nat. Commun.* **2022**, *13* (1), 1−9.
(33) Delafontaine, L.; Murphy, E.; Guo, S.; Liu, Y.; Asset, T.; Huang, Y.; Chen, J.; Zenyuk, I. V.; Pan, X.; Atanassov, P. Synergistic Electrocatalytic Syngas Production from Carbon Dioxide by Bi-Metallic Atomically Dispersed Catalysts. *ChemElectroChem* **2022**, *9* (17), e202200647.
(34) Murphy, E.; Liu, Y.; Matanovic, I.; Guo, S.; Tieu, P.; Huang, Y.; Ly, A.; Das, S.; Zenyuk, I.; Pan, X.; Spoerke, E.; Atanassov, P. Highly Durable and Selective Fe- and Mo-Based Atomically Dispersed Electrocatalysts for Nitrate Reduction to Ammonia via Distinct and Synergized NO 2 - Pathways. *ACS Catal.* **2022**, *12* (11), 6651−6662.
(35) Murphy, E.; Sun, B.; Rüscher, M.; Liu, Y.; Zang, W.; Guo, S.; Chen, Y.; Hejral, U.; Huang, Y.; Ly, A.; Zenyuk, I. V.; Pan, X.; Timoshenko, J.; Cuenya, B. R.; Spoerke, E. D.; Atanassov, P. Synergizing Fe_2O_3 Nanoparticles on Single Atom Fe-N-C for Nitrate Reduction to Ammonia at Industrial Current Densities. *Adv. Mater.* **2024**, *2401133*, 202401133.
(36) Feng, Q.; Wang, X.; Klingenhof, M.; Heggen, M.; Strasser, P. Low-Pt NiNC-Supported PtNi Nanoalloy Oxygen Reduction Reaction Electrocatalysts—In Situ Tracking of the Atomic Alloying Process. *Angew. Chemie - Int. Ed.* **2022**, *61* (36), e202203728.
(37) Chen, M.; Li, C.; Zhang, B.; Zeng, Y.; Karakalos, S.; Hwang, S.; Xie, J.; Wu, G. High-Platinum-Content Catalysts on Atomically Dispersed and Nitrogen Coordinated Single Manganese Site Carbons for Heavy-Duty Fuel Cells. *J. Electrochem. Soc.* **2022**, *169* (3), 034510.
(38) Qiao, Z.; Wang, C.; Li, C.; Zeng, Y.; Hwang, S.; Li, B.; Karakalos, S.; Park, J.; Kropf, A. J.; Wegener, E. C.; Gong, Q.; Xu, H.; Wang, G.; Myers, D. J.; Xie, J.; Spendelow, J. S.; Wu, G. Atomically Dispersed Single Iron Sites for Promoting Pt and Pt3Co Fuel Cell Catalysts: Performance and Durability Improvements. *Energy Environ. Sci.* **2021**, *14* (9), 4948−4960.
(39) Murphy, E.; Liu, Y.; Matanovic, I.; Ruscher, M.; Huang, Y.; Ly, A.; Guo, S.; Zang, W.; Yan, X.; Martini, A.; Timoshenko, J.; Cuenya, B. R.; Zenyuk, I. V.; Pan, X.; Spoerke, E. D.; Atanassov, P. Atanassov Plamen. Elucidating Electrochemical Nitrate and Nitrite Reduction over Atomically-Dispersed Transition Metal Sites. *Nat. Commun.* **2023**, *14* (2), 4−6.
(40) Pylypenko, S.; Mukherjee, S.; Olson, T. S.; Atanassov, P. Non-Platinum Oxygen Reduction Electrocatalysts Based on Pyrolyzed Transition Metal Macrocycles. *Electrochim. Acta* **2008**, *53* (27), 7875−7883.
(41) Serov, A.; Artyushkova, K.; Niangar, E.; Wang, C.; Dale, N.; Jaouen, F.; Sougrati, M. T.; Jia, Q.; Mukerjee, S.; Atanassov, P. Nano-Structured Non-Platinum Catalysts for Automotive Fuel Cell Application. *Nano Energy* **2015**, *16*, 293−300.
(42) Workman, M. J.; Serov, A.; Tsui, L. K.; Atanassov, P.; Artyushkova, K. Fe-N-C Catalyst Graphitic Layer Structure and Fuel Cell Performance. *ACS Energy Lett.* **2017**, *2* (7), 1489−1493.
(43) Bates, J. S.; Martinez, J. J.; Hall, M. N.; Al-Omari, A. A.; Murphy, E.; Zeng, Y.; Luo, F.; Primbs, M.; Menga, D.; Bibent, N.; Sougrati, M. T.; Wagner, F. E.; Atanassov, P.; Wu, G.; Strasser, P.; Fellinger, T.-P.; Jaouen, F.; Root, T. W.; Stahl, S. S. Chemical Kinetic Method for Active-Site Quantification in Fe-N-C Catalysts and Correlation with Molecular Probe and Spectroscopic Site-Counting Methods. *J. Am. Chem. Soc.* **2023**, *145*, 26222−26237.
(44) Primbs, M.; Sun, Y.; Roy, A.; Malko, D.; Mehmood, A.; Sougrati, M. T.; Blanchard, P. Y.; Granozzi, G.; Kosmala, T.; Daniel, G.; Atanassov, P.; Sharman, J.; Durante, C.; Kucernak, A.; Jones, D.; Jaouen, F.; Strasser, P. Establishing Reactivity Descriptors for Platinum Group Metal (PGM)-Free Fe-N-C Catalysts for PEM Fuel Cells. *Energy Environ. Sci.* **2020**, *13* (8), 2480−2500.
(45) Huang, Y.; Chen, Y.; Xu, M.; Asset, T.; Tieu, P.; Gili, A.; Kulkarni, D.; De Andrade, V.; De Carlo, F.; Barnard, H. S.; Doran, A.; Parkinson, D. Y.; Pan, X.; Atanassov, P.; Zenyuk, I. V. Catalysts by Pyrolysis: Direct Observation of Chemical and Morphological Transformations Leading to Transition Metal-Nitrogen-Carbon Materials. *Mater. Today* **2021**, *47* (August), 53−68.

https://doi.org/10.1021/acscatal.4c02717
ACS Catal. 2024, 14, 9797−9811

(46) Chen, Y.; Huang, Y.; Xu, M.; Asset, T.; Yan, X.; Artyushkova, K.; Kodali, M.; Murphy, E.; Ly, A.; Pan, X.; Zenyuk, I. V.; Atanassov, P. Catalysts by Pyrolysis: Direct Observation of Transformations during Re-Pyrolysis of Transition Metal-Nitrogen-Carbon Materials Leading to State-of-the-Art Platinum Group Metal-Free Electrocatalyst. *Mater. Today* **2022**, *53* (March), 58−70.
(47) Hanifpour, F.; Sveinbjörnsson, A.; Canales, C. P.; Skulason, E.; Flosadottir, H. D. Preparation of Nafion Membranes for Reproducible Ammonia Quantification in Nitrogen Reduction Reaction Experiments. *Angew. Chem.* **2020**, *132* (51), 23138−23142.
(48) Zou, H.; Rong, W.; Wei, S.; Ji, Y.; Duan, L. Regulating Kinetics and Thermodynamics of Electrochemical Nitrogen Reduction with Metal Single-Atom Catalysts in a Pressurized Electrolyser. *Proc. Natl. Acad. Sci. U. S. A.* **2020**, *117* (47), 29462−29468.
(49) Nature Communications. A Checklist for Reproducibility in Electrochemical Nitrogen Fixation. *Nat. Commun.* **2022**, *13* (1), 4642.
(50) Xiong, Y.; Wang, Y.; Zhou, J.; Liu, F.; Hao, F.; Fan, Z. Electrochemical Nitrate Reduction: Ammonia Synthesis and the Beyond. *Adv. Mater.* **2024**, *36*, 2304021.
(51) Wang, Y.; Shao, M. Theoretical Screening of Transition Metal-N4-Doped Graphene for Electroreduction of Nitrate. *ACS Catal.* **2022**, *12* (9), 5407−5415.
(52) Niu, H.; Zhang, Z.; Wang, X.; Wan, X.; Shao, C.; Guo, Y. Theoretical Insights into the Mechanism of Selective Nitrate-to-Ammonia Electroreduction on Single-Atom Catalysts. *Adv. Funct. Mater.* **2021**, *31* (11), 1−8.
(53) Chen, F. Y.; Wu, Z. Y.; Gupta, S.; Rivera, D. J.; Lambeets, S. V.; Pecaut, S.; Kim, J. Y. T.; Zhu, P.; Finfrock, Y. Z.; Meira, D. M.; King, G.; Gao, G.; Xu, W.; Cullen, D. A.; Zhou, H.; Han, Y.; Perea, D. E.; Muhich, C. L.; Wang, H. Efficient Conversion of Low-Concentration Nitrate Sources into Ammonia on a Ru-Dispersed Cu Nanowire Electrocatalyst. *Nat. Nanotechnol.* **2022**, *17* (7), 759−767.
(54) Yang, J.; Qi, H.; Li, A.; Liu, X.; Yang, X.; Zhang, S.; Zhao, Q.; Jiang, Q.; Su, Y.; Zhang, L.; Li, J. F.; Tian, Z. Q.; Liu, W.; Wang, A.; Zhang, T. Potential-Driven Restructuring of Cu Single Atoms to Nanoparticles for Boosting the Electrochemical Reduction of Nitrate to Ammonia. *J. Am. Chem. Soc.* **2022**, *144* (27), 12062−12071.
(55) Hollevoet, L.; Vervloessem, E.; Gorbanev, Y.; Nikiforov, A.; De Geyter, N.; Bogaerts, A.; Martens, J. A. Energy-Efficient Small-Scale Ammonia Synthesis Process with Plasma-Enabled Nitrogen Oxidation and Catalytic Reduction of Adsorbed NOx. *ChemSusChem* **2022**, *15* (10), e202102526.
(56) Li, L.; Tang, C.; Cui, X.; Zheng, Y.; Wang, X.; Xu, H.; Zhang, S.; Shao, T.; Davey, K.; Qiao, S. Z. Efficient Nitrogen Fixation to Ammonia through Integration of Plasma Oxidation with Electrocatalytic Reduction. *Angew. Chemie - Int. Ed.* **2021**, *60* (25), 14131−14137.
(57) Muzammil, I.; Kim, Y. N.; Kang, H.; Dinh, D. K.; Choi, S.; Jung, C.; Song, Y. H.; Kim, E.; Kim, J. M.; Lee, D. H. Plasma Catalyst-Integrated System for Ammonia Production from H2O and N2at Atmospheric Pressure. *ACS Energy Lett.* **2021**, *6*, 3004−3010.
(58) Sun, J.; Alam, D.; Daiyan, R.; Masood, H.; Zhang, T.; Zhou, R.; Cullen, P. J.; Lovell, E. C.; Jalili, A.; Amal, R. A Hybrid Plasma Electrocatalytic Process for Sustainable Ammonia Production. *Energy Environ. Sci.* **2021**, *14* (2), 865−872.
(59) Zhou, D.; Zhou, R.; Zhou, R.; Liu, B.; Zhang, T.; Xian, Y.; Cullen, P. J.; Lu, X.; Ostrikov, K. Sustainable Ammonia Production by Non-Thermal Plasmas: Status, Mechanisms, and Opportunities. *Chem. Eng. J.* **2021**, *421* (P1), 129544.
(60) Zhu, T.; Chen, Q.; Liao, P.; Duan, W.; Liang, S.; Yan, Z.; Feng, C. Single-Atom Cu Catalysts for Enhanced Electrocatalytic Nitrate Reduction with Significant Alleviation of Nitrite Production. *Small* **2020**, *16* (49), 1−11.
(61) Zhang, W. Da; Dong, H.; Zhou, L.; Xu, H.; Wang, H. R.; Yan, X.; Jiang, Y.; Zhang, J.; Gu, Z. G. Fe Single-Atom Catalysts with Pre-Organized Coordination Structure for Efficient Electrochemical Nitrate Reduction to Ammonia. *Appl. Catal. B Environ.* **2022**, *317* (May), 121750.
(62) Xu, M.; Xie, Q.; Duan, D.; Zhang, Y.; Zhou, Y.; Zhou, H.; Li, X.; Wang, Y.; Gao, P.; Ye, W. Atomically Dispersed Cu Sites on Dual-Mesoporous N-Doped Carbon for Efficient Ammonia Electrosynthesis from Nitrate. *ChemSusChem* **2022**, *15* (11), e202200231.
(63) Cheng, X. F.; He, J. H.; Ji, H. Q.; Zhang, H. Y.; Cao, Q.; Sun, W. J.; Yan, C. L.; Lu, J. M. Coordination Symmetry Breaking of Single-Atom Catalysts for Robust and Efficient Nitrate Electroreduction to Ammonia. *Adv. Mater.* **2022**, *34* (36), 1−10.
(64) Wang, Y.; Yin, H.; Dong, F.; Zhao, X.; Qu, Y.; Wang, L.; Peng, Y.; Wang, D.; Fang, W.; Li, J. N-Coordinated Cu-Ni Dual-Single-Atom Catalyst for Highly Selective Electrocatalytic Reduction of Nitrate to Ammonia. *Small* **2023**, *19*, 2207695.
(65) Wang, Y.; Xu, A.; Wang, Z.; Huang, L.; Li, J.; Li, F.; Wicks, J.; Luo, M.; Nam, D. H.; Tan, C. S.; Ding, Y.; Wu, J.; Lum, Y.; Dinh, C. T.; Sinton, D.; Zheng, G.; Sargent, E. H. Enhanced Nitrate-to-Ammonia Activity on Copper-Nickel Alloys via Tuning of Intermediate Adsorption. *J. Am. Chem. Soc.* **2020**, *142* (12), 5702−5708.
(66) Murphy, E.; Sun, B.; Ruscher, M.; Liu, Y.; Zang, W.; Guo, S.; Chen, Y.-H.; Hejral, U.; Huang, Y.; Ly, A.; Zenyuk, I. V.; Pan, X.; Timoshenko, J.; Cuenya, B. R.; Spoerke, E. D.; Atanassov, P. Elucidating electrochemical nitrate and nitrite reduction over atomically-dispersed transition metal sites. *ChemRxiv* November 9, 2022, ver. 1. .
(67) Guo, P.; Liu, B.; Dai, Y. K.; Gong, X. F.; Xia, Y. F.; Zhang, Y. L.; Liu, B.; Zhao, L.; Sui, X. L.; Wang, Z. B. Coupling Fine Pt Nanoparticles and Co-Nx Moiety as a Synergistic Bi-Active Site Catalyst for Oxygen Reduction Reaction in Acid Media. *J. Colloid Interface Sci.* **2022**, *613*, 276−284.
(68) Ly, A.; Murphy, E.; Wang, H.; Huang, Y.; Ferro, G.; Guo, S.; Asset, T.; Liu, Y.; Zenyuk, I. V.; Atanassov, P. Electrochemical Trends of a Hybrid Platinum and Metal-Nitrogen-Carbon Catalyst Library for the Oxygen Reduction Reaction. *EES Catal.* **2024**, *2* (2), 624−637.
(69) Cao, Y.; Yuan, S.; Meng, L.; Wang, Y.; Hai, Y.; Su, S.; Ding, W.; Liu, Z.; Li, X.; Luo, M. Recent Advances in Electrocatalytic Nitrate Reduction to Ammonia: Mechanism Insight and Catalyst Design. *ACS Sustain. Chem. Eng.* **2023**, *11*, 7965.
(70) Chen, W.; Yang, X.; Chen, Z.; Ou, Z.; Hu, J.; Xu, Y.; Li, Y.; Ren, X.; Ye, S.; Qiu, J.; Liu, J.; Zhang, Q. Emerging Applications, Developments, Prospects, and Challenges of Electrochemical Nitrate-to-Ammonia Conversion. *Adv. Funct. Mater.* **2023**.
(71) International Energy Agency (IEA). Ammonia Technology Roadmap. Towards More Sustainable Nitrogen Fertiliser Production. IEA: Paris, France, 2021; https://www.iea.org/reports/ammonia-technology-roadmap.
(72) Lv, C.; Zhong, L.; Liu, H.; Fang, Z.; Yan, C.; Chen, M.; Kong, Y.; Lee, C.; Liu, D.; Li, S.; Liu, J.; Song, L.; Chen, G.; Yan, Q.; Yu, G. Selective Electrocatalytic Synthesis of Urea with Nitrate and Carbon Dioxide. *Nat. Sustain.* **2021**, *4* (10), 868−876.
(73) Krzywda, P.; Paradelo Rodríguez, A.; Benes, N. E.; Mei, B. T.; Mul, G. Carbon-Nitrogen Bond Formation on Cu Electrodes during CO2 Reduction in NO3- Solution. *Appl. Catal. B: Environ.* **2022**, *316*, 121512.
(74) Meng, N.; Huang, Y.; Liu, Y.; Yu, Y.; Zhang, B. Electrosynthesis of Urea from Nitrite and CO2 over Oxygen Vacancy-Rich ZnO Porous Nanosheets. *Cell Reports Phys. Sci.* **2021**, *2* (3), 100378.
(75) Yuan, M.; Chen, J.; Bai, Y.; Liu, Z.; Zhang, J.; Zhao, T.; Shi, Q.; Li, S.; Wang, X.; Zhang, G. Electrochemical C-N Coupling with Perovskite Hybrids toward Efficient Urea Synthesis. *Chem. Sci.* **2021**, *12* (17), 6048−6058.
(76) Huang, Y.; Wang, Y.; Liu, Y.; Ma, A.; Gui, J.; Zhang, C.; Yu, Y.; Zhang, B. Unveiling the Quantification Minefield in Electrocatalytic Urea Synthesis. *Chem. Eng. J.* **2023**, *453* (P1), 139836.
(77) Chen, S.; Lin, S.; Ding, L.; Wang, H. Modified Diacetylmonoxime-Thiosemicarbazide Detection Protocol for Accurate Quantification of Urea. *Small Methods* **2023**, *7* (9), 2300003.
(78) Leverett, J.; Tran-Phu, T.; Yuwono, J. A.; Kumar, P.; Kim, C.; Zhai, Q.; Han, C.; Qu, J.; Cairney, J.; Simonov, A. N.; Hocking, R. K.; Dai, L.; Daiyan, R.; Amal, R. Tuning the Coordination Structure of

https://doi.org/10.1021/acscatal.4c02717
ACS Catal. 2024, 14, 9797−9811

Cu-N-C Single Atom Catalysts for Simultaneous Electrochemical Reduction of CO2 and NO3- to Urea. *Adv. Energy Mater.* **2022**, *12* (32), 2201500.
(79) Zhao, T.; Chen, K.; Xu, X.; Li, X.; Zhao, X.; Cai, Q.; Chu, K.; Zhao, J. Homonuclear Dual-Atom Catalysts Embedded on N-Doped Graphene for Highly Efficient Nitrate Reduction to Ammonia: From Theoretical Prediction to Experimental Validation. *Appl. Catal. B Environ.* **2023**, *339* (July), 123156.
(80) Lv, Z.; Zhao, L.; Zhou, S.; Wang, M.; Xu, W.; Lai, J.; Wang, L. CuCo DAC Used to Change the Hydrogenation Sequence for Efficient Electrochemical C-N Coupling. *Appl. Catal. B Environ.* **2024**, *351* (February), 124003.
(81) Li, Y.; Zheng, S.; Liu, H.; Xiong, Q.; Yi, H.; Yang, H.; Mei, Z.; Zhao, Q.; Yin, Z. W.; Huang, M.; Lin, Y.; Lai, W.; Dou, S. X.; Pan, F.; Li, S. Sequential Co-Reduction of Nitrate and Carbon Dioxide Enables Selective Urea Electrosynthesis. *Nat. Commun.* **2024**, *15* (1), 176.
(82) Zhu, C.; Geng, Y.; Yao, X.; Zhu, G.; Su, Z.; Zhang, M. Fascinating Electrocatalysts with Dispersed Di-Metals in MN3-M′N4Moiety as Two Active Sites Separately for N2 and CO2 Reduction Reactions and Jointly for C-N Coupling and Urea Production. *Small Methods* **2023**, *7* (3), 1−14.
(83) Bates, J. S.; Khamespanah, F.; Cullen, D. A.; Al-Omari, A. A.; Hopkins, M. N.; Martinez, J. J.; Root, T. W.; Stahl, S. S. Molecular Catalyst Synthesis Strategies to Prepare Atomically Dispersed Fe-NC Heterogeneous Catalysts. *J. Am. Chem. Soc.* **2022**, *144* (41), 18797−18802.
(84) Jouny, M.; Lv, J. J.; Cheng, T.; Ko, B. H.; Zhu, J. J.; Goddard, W. A.; Jiao, F. Formation of Carbon-Nitrogen Bonds in Carbon Monoxide Electrolysis. *Nat. Chem.* **2019**, *11* (9), 846−851.

https://doi.org/10.1021/acscatal.4c02717
ACS Catal. 2024, 14, 9797−9811